Sainsbury Wellcome Centre

Sept. 30, 2019

Methods for recording neuronal activity

Prof. Tom Otis
t.otis@ucl.ac.uk

From ‘animal electricity’… to how nerves work

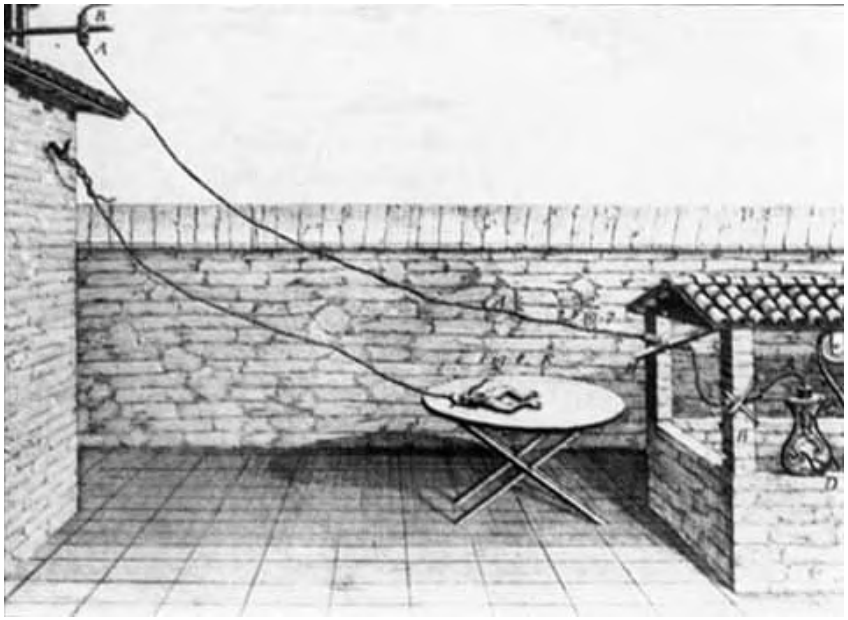

Galvani, 1780

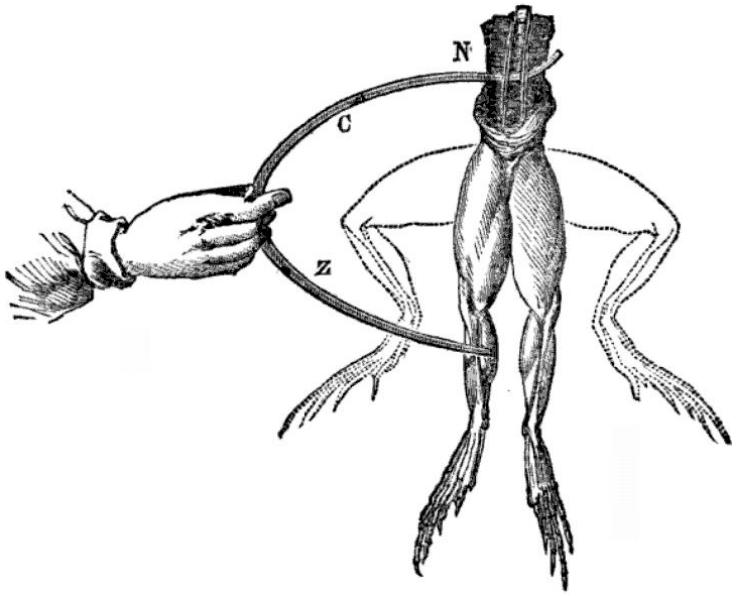

Galvani, 1791

Helmholtz's measurements of nerve conduction velocity

Hermann von Helmholtz

Devices to measure time intervals:

Claude Pouillet's bullet velocity device, 1844

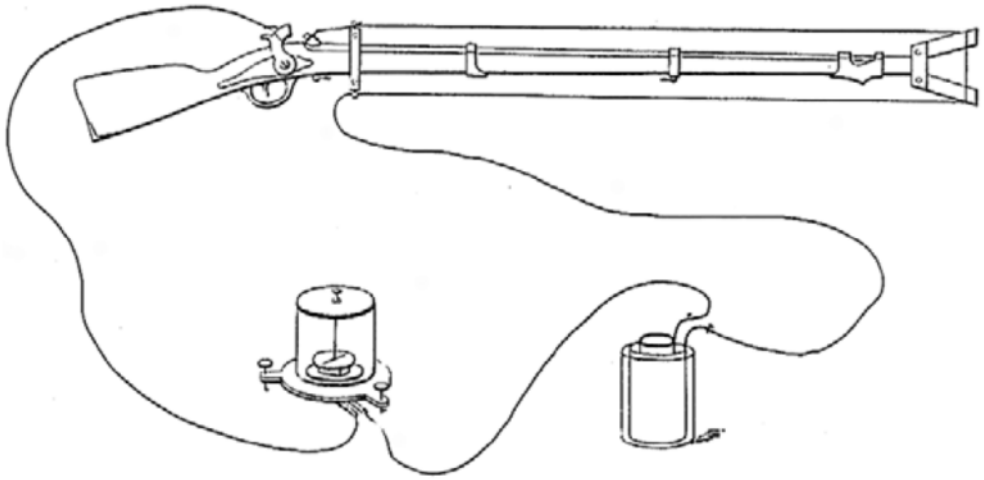

Helmholtz's design for measuring nerve conduction velocity, c 1848

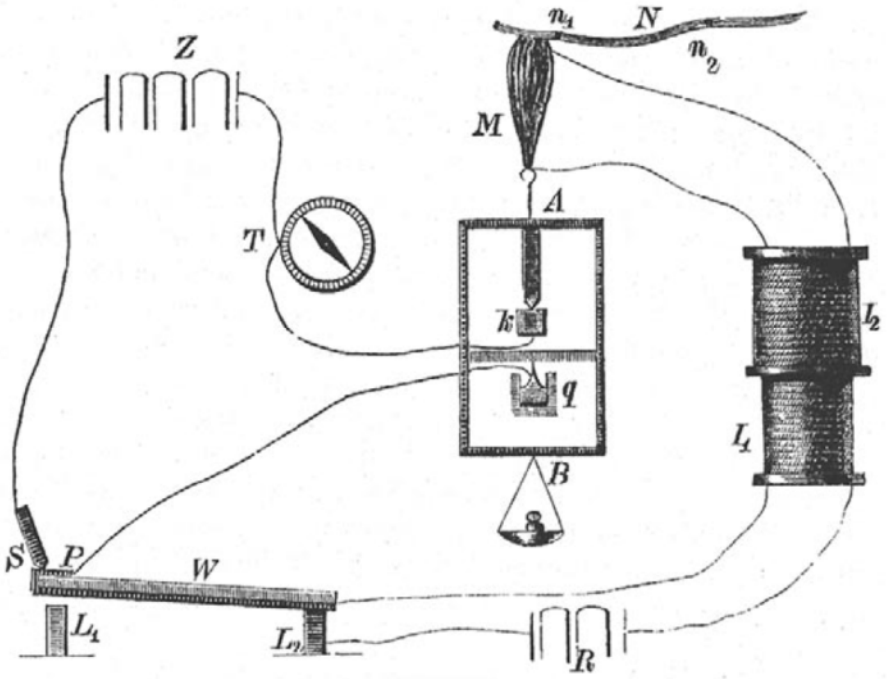

from Schnmidgen, *Endeavour*, 26:142 (2002)

Willem Einthoven's string galvanometer

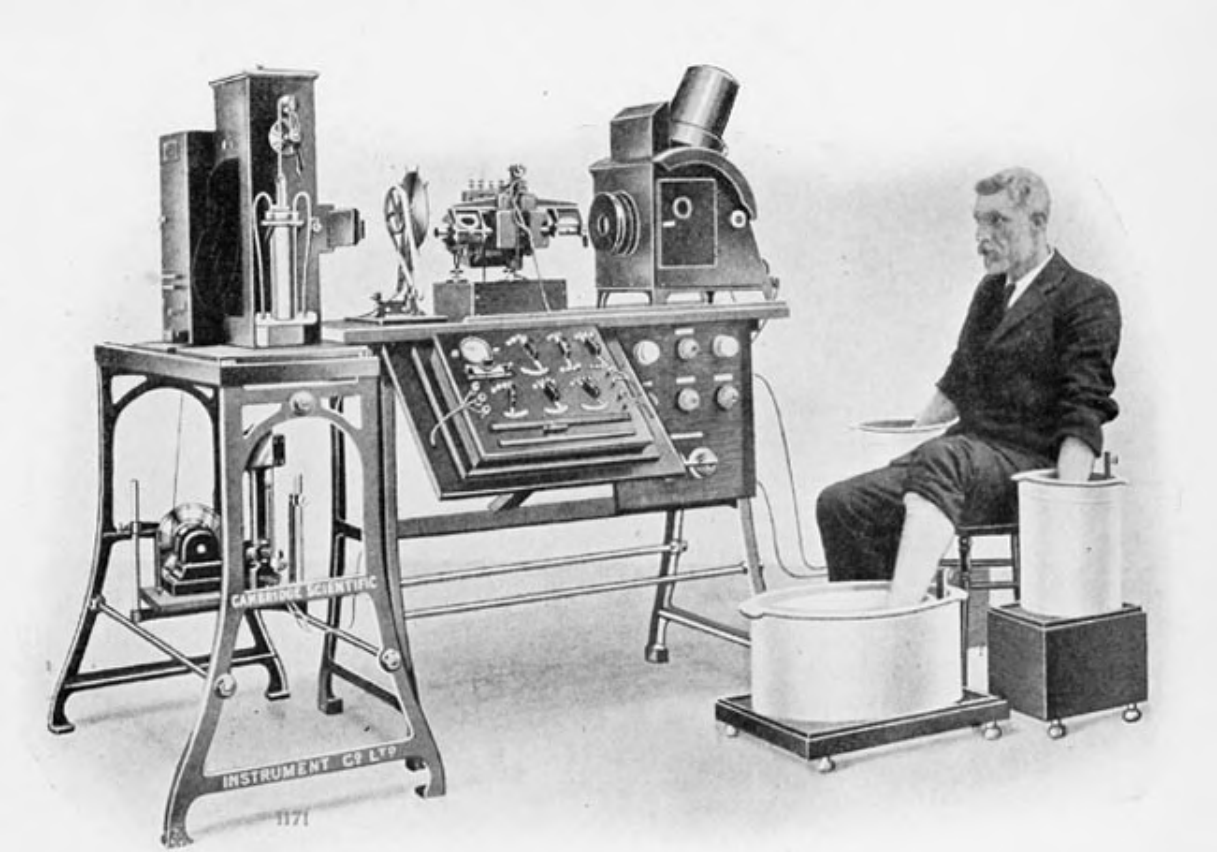

PHOTOGRAPH OF A COMPLETE ELECTROCARDIOGRAPH, SHOWING THE MANNER IN WHICH THE ELECTRODES ARE ATTACHED TO THE PATIENT, IN THIS CASE THE HANDS AND ONE FOOT BEING IMMERSED IN JARS OF SALT SOLUTION

Willem Einthoven

First electrical recordings of a nerve impulse

frog sciatic nerve

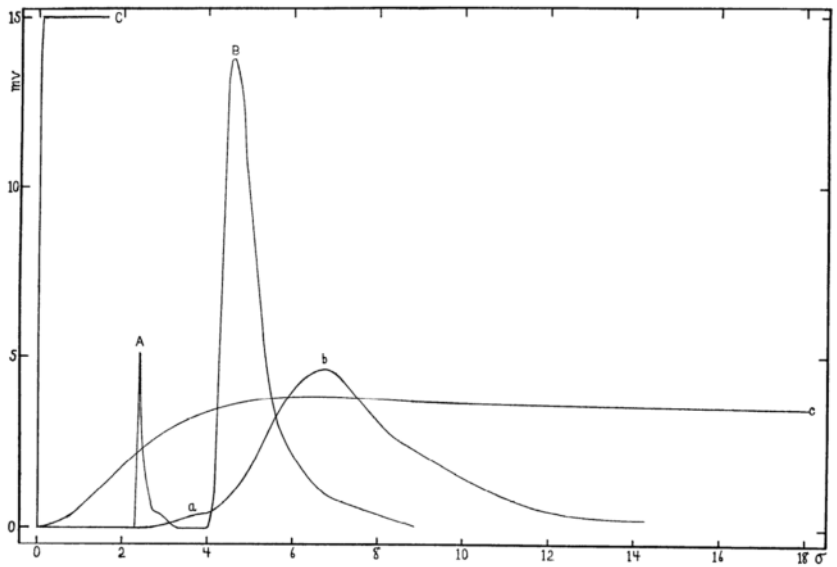

Fig. 3. The action currents of the bull frog sciatic, as recorded by the Braun tube and string galvanometer, plotted in rectangular linear coördinates. *A, B, C,* Braun tube records; *a, b, c,* string galvanometer records. *A, a,* shock; *B, b,* action current; *C,* calibration with a constant current of 15 mv.; *c,* with one of 3.75 mv.

American J. Physiol., 1922

Herbert Gasser

Joseph Erlanger

First recordings of light-evoked activity in optic nerve

Conger eel optic nerve

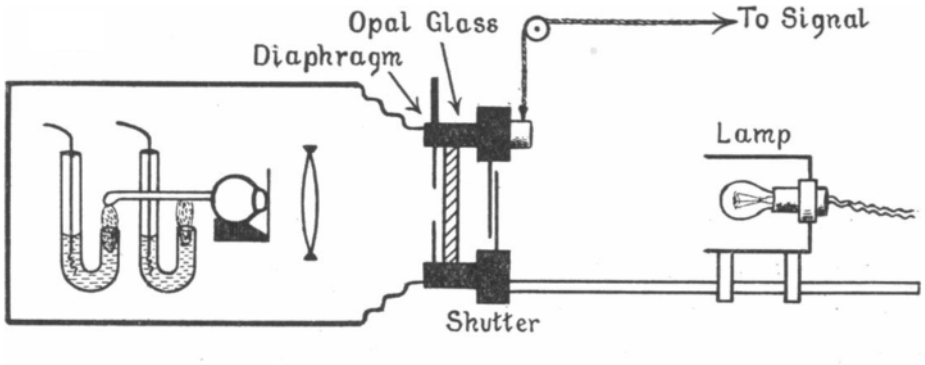

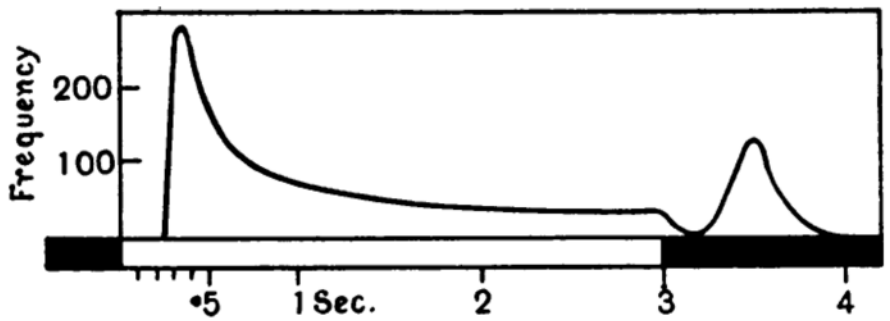

Lord Edgar Douglas Adrian

J. Physiology, 1927

"I had arranged electrodes on the optic nerve of a toad in connection with some experiments on the retina. The room was nearly dark and I was puzzled to hear repeated noises in the loudspeaker attached to the amplifier, noises indicating that a great deal of impulse activity was going on. It was not until I compared the noises with my own movements around the room that I realised I was in the field of vision of the toad's eye and that it was signalling what I was doing."

Mechanism of the nerve impulse

Squid giant axon

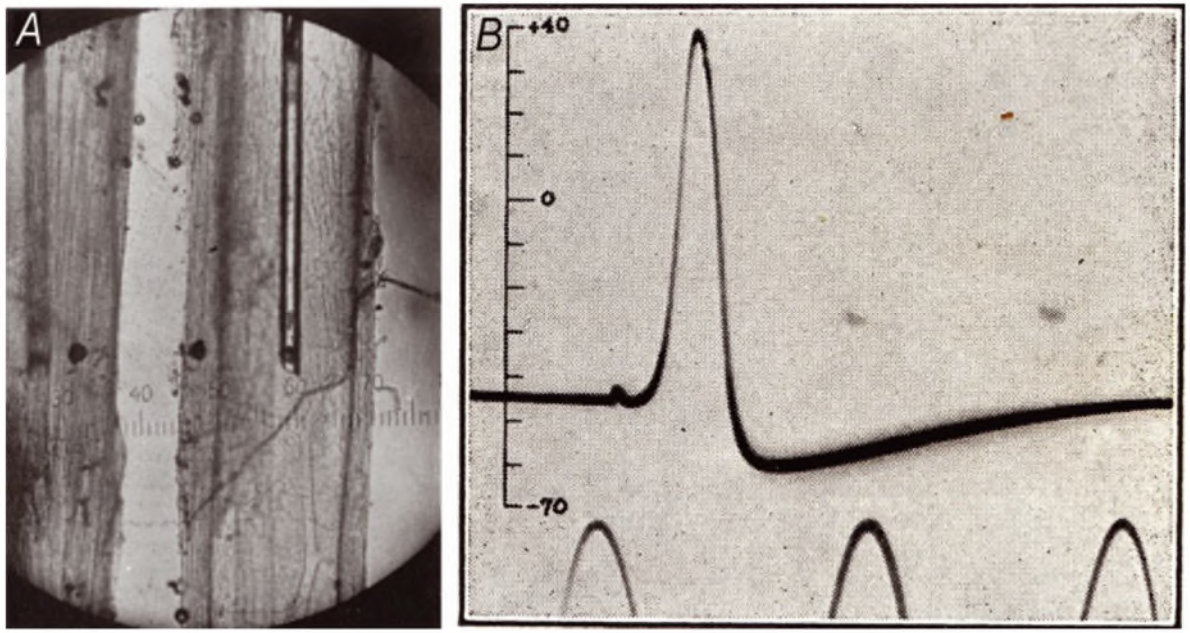

Nature, 1939

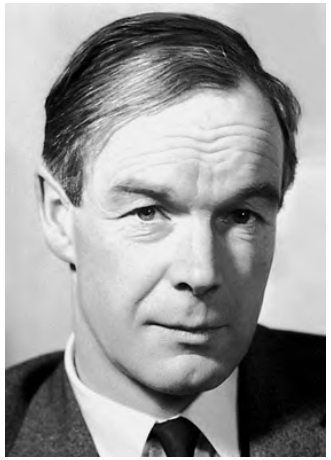

Alan Hodgkin

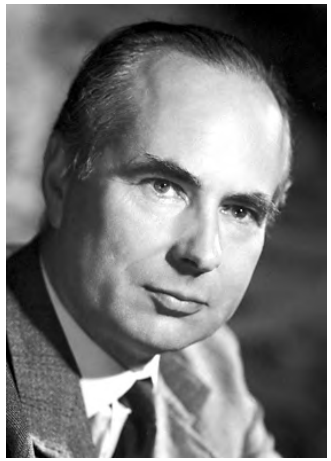

Andrew Huxley

Hodgkin Huxley model of the action potential

http://nerve.bsd.uchicago.edu/

Fig.1

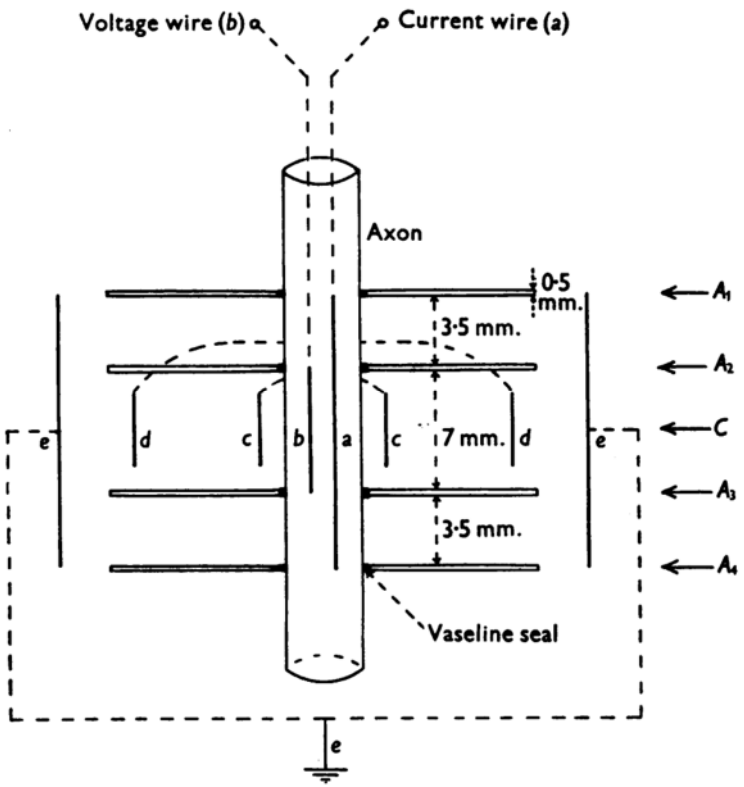

Fig.4

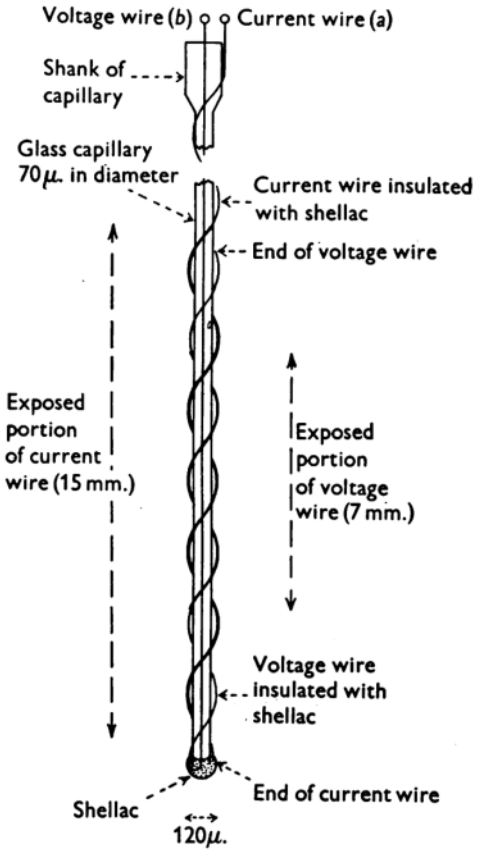

Hodgkin, Huxley, and Katz, J. Physiol., 1952

Intracellular measurements with a microelectrode

Ag/AgCl wires are standard in physiological contexts due to their excellent bidirectional ionic mobility, stability

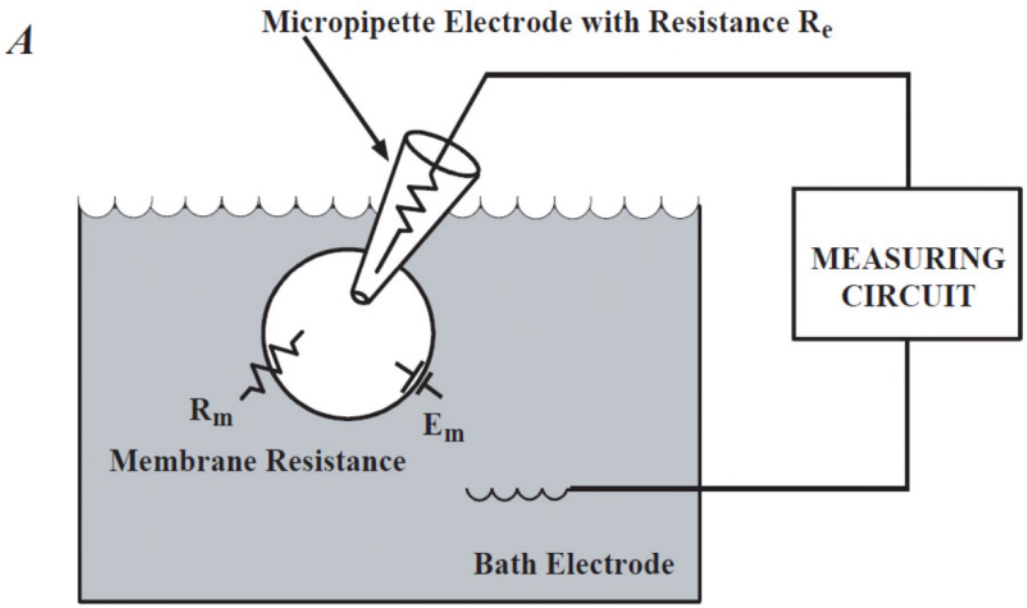

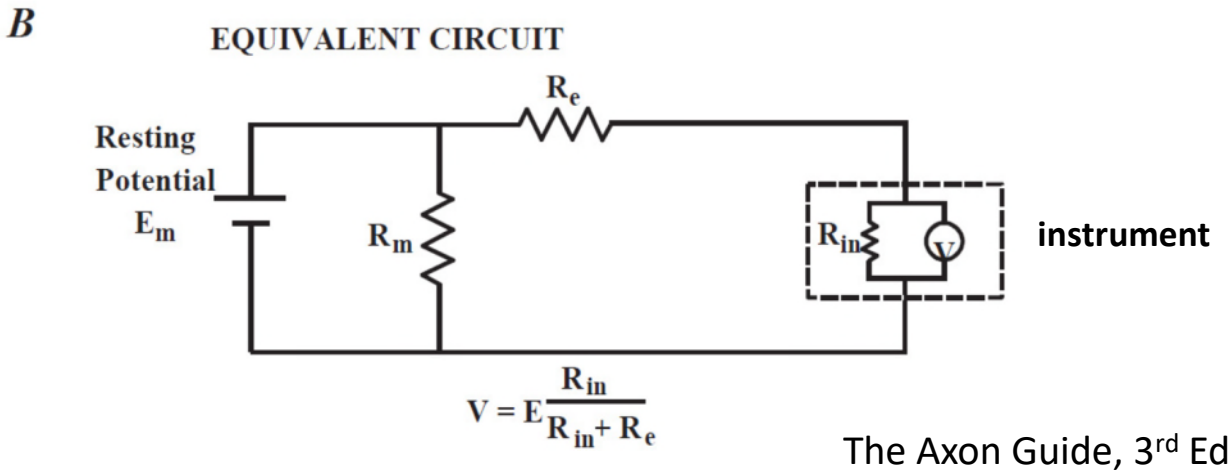

The Axon Guide, 3rd Ed.

Microelectrode methods for intracellular recording

‘sharp’ microelectrode

3 M KCl, 3 M K Acetate
80-100 MΩ

whole-cell patch pipette

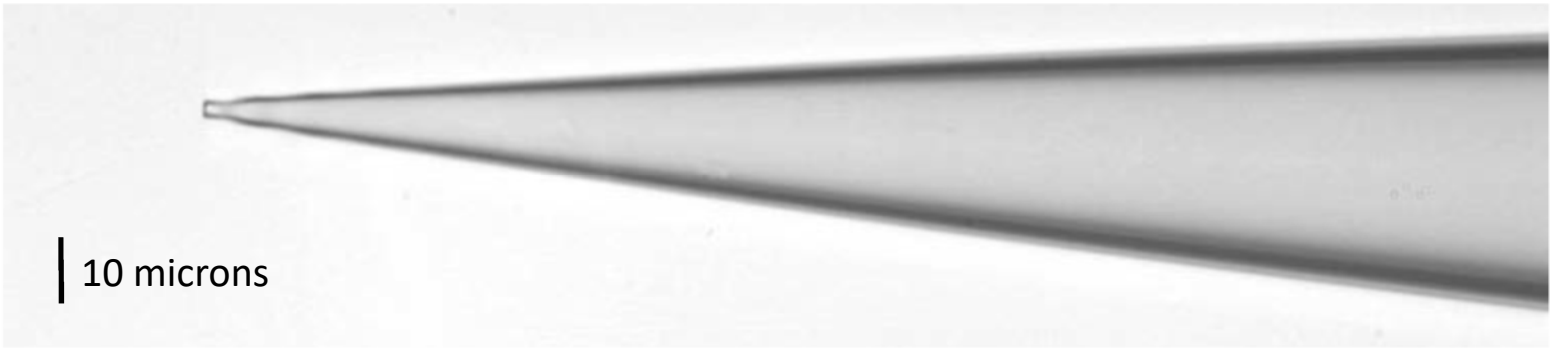

physiological internal
e.g. 130 K $MeSO_4$
2-5 MΩ

Patch clamping

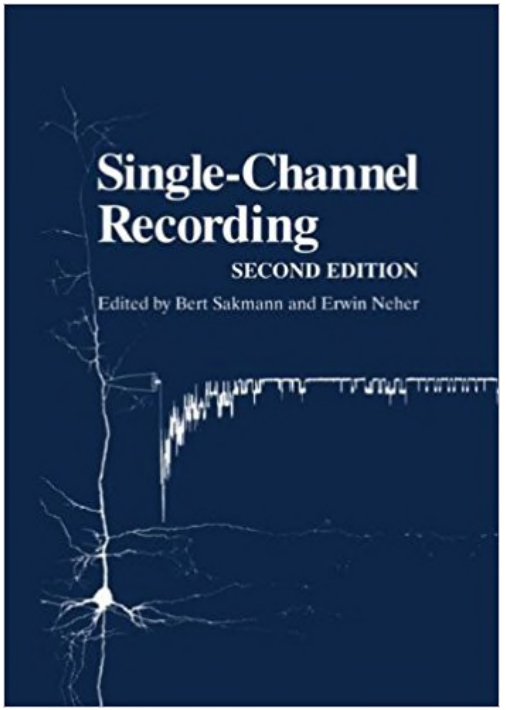

https://youtu.be/M3xN4Ihmt7U

from Purves et al, Neuroscience 5th Ed. 2012

Microelectrode methods for intracellular recording

Rat dentate gyrus granule cells

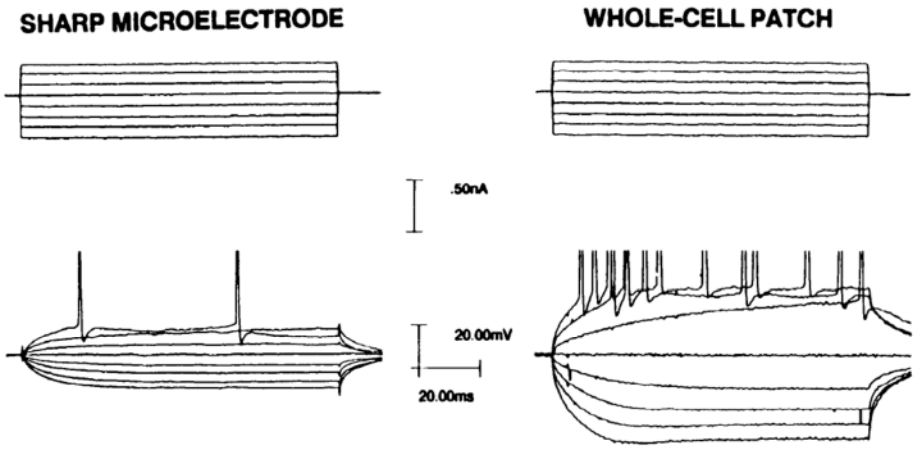

FIG. 4. Comparison of membrane voltage responses to current steps in GCs recorded with sharp electrode vs. whole-cell patch electrode. Sharp electrode filled with 3 M potassium acetate. The differences in R_N and τ_m can be appreciated by visual inspection of the records. Spike threshold is similar for the 2 recording methods.

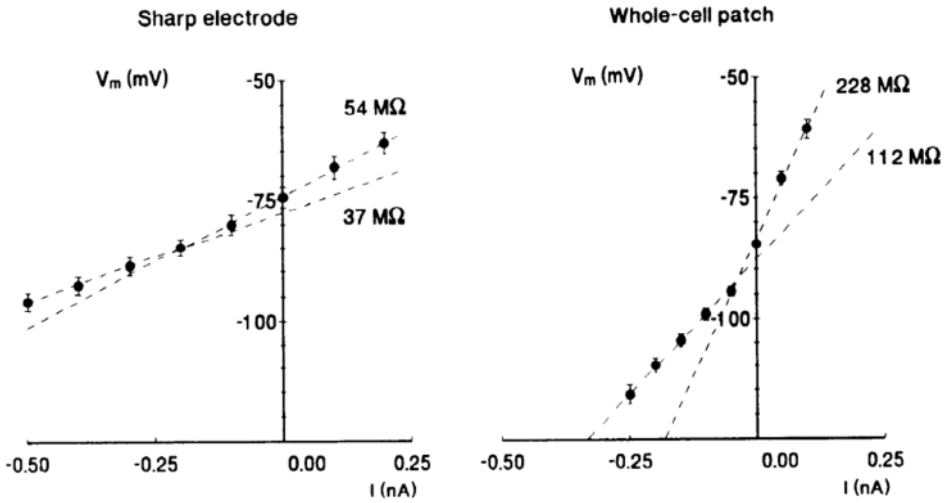

FIG. 5. Membrane voltage vs. injected current for 31 GCs recorded in whole-cell method and 10 GCs recorded with sharp electrodes; points are means ± SE. Voltage was determined 180 ms after start of current pulse. Error bars indicate SE. Lines are fitted by least-squares method. Regions of linearity determined by eye.

Staley et al., J. Neurophysiol. 1992

Recording from populations of single neurons: tetrodes

Thomas Recording tetrode

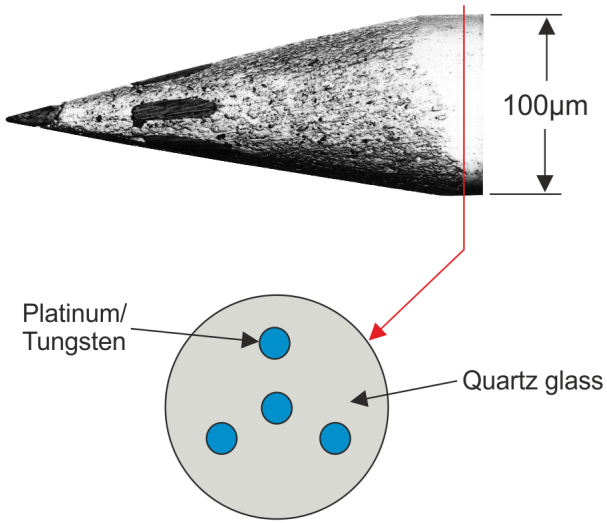

see Recce & O'Keefe, 1989

microwire tetrode

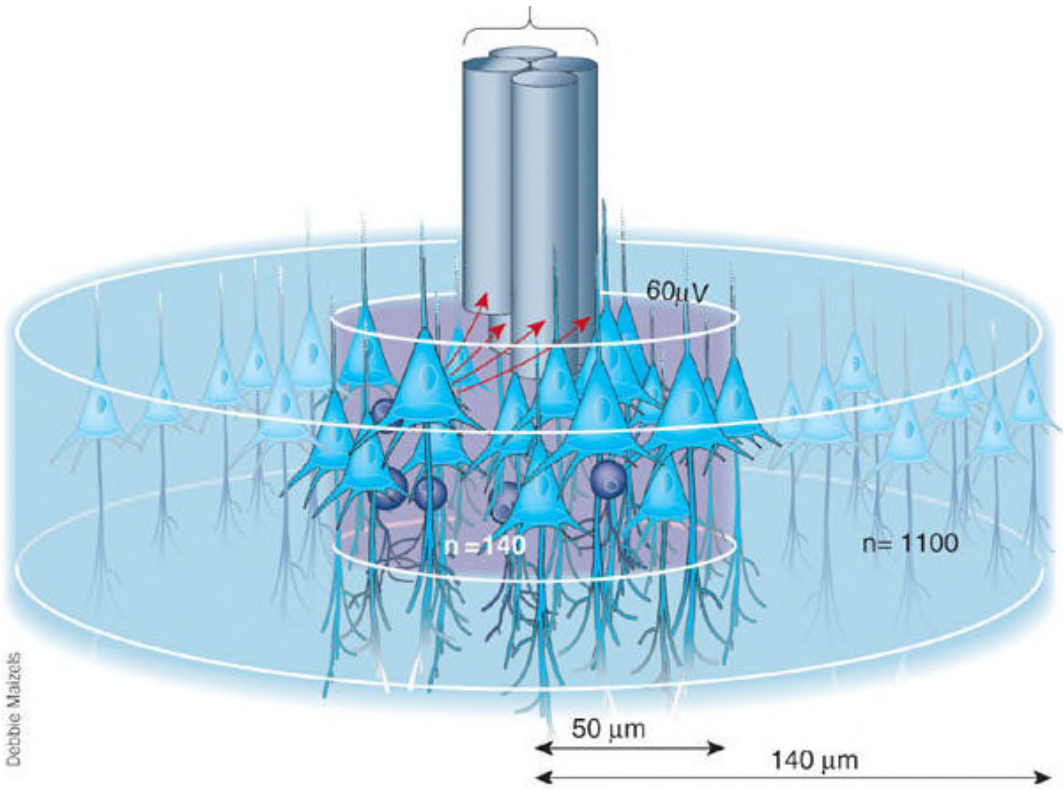

Buzsáki, *Nat. Neurosci.* 2004

Recording from populations of single neurons: tetrodes

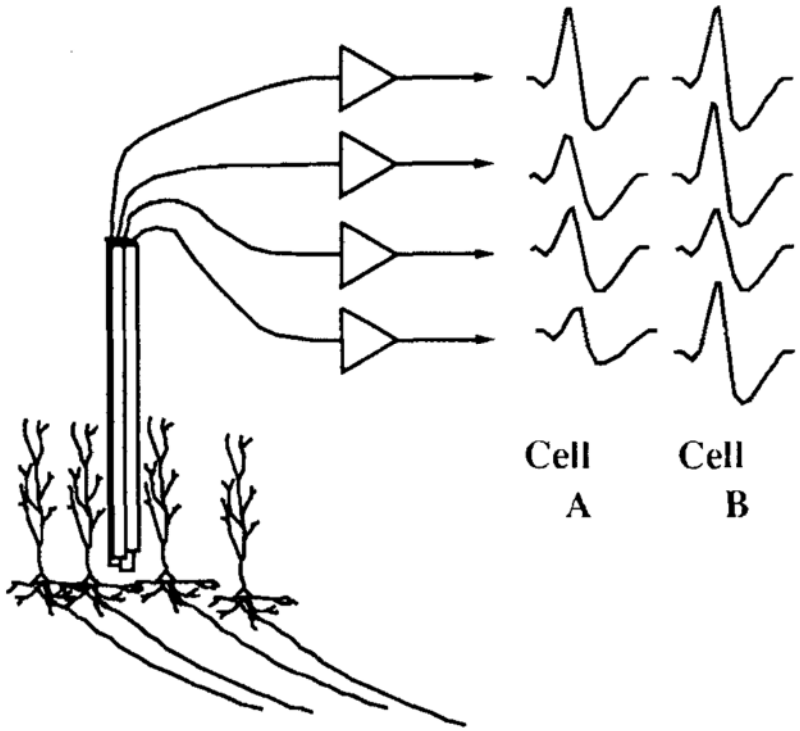

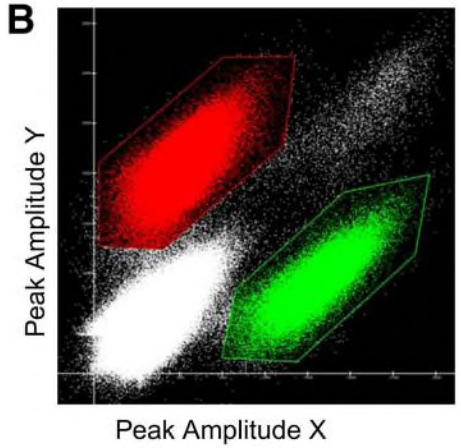

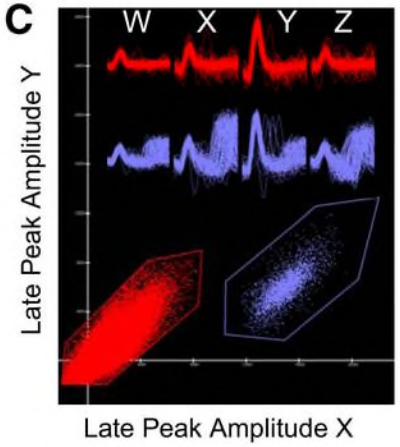

O'Keefe & Recce, 1993

Halverson et al., J. Neurosci. 35:7182-32, 2015

Neuropixel probes

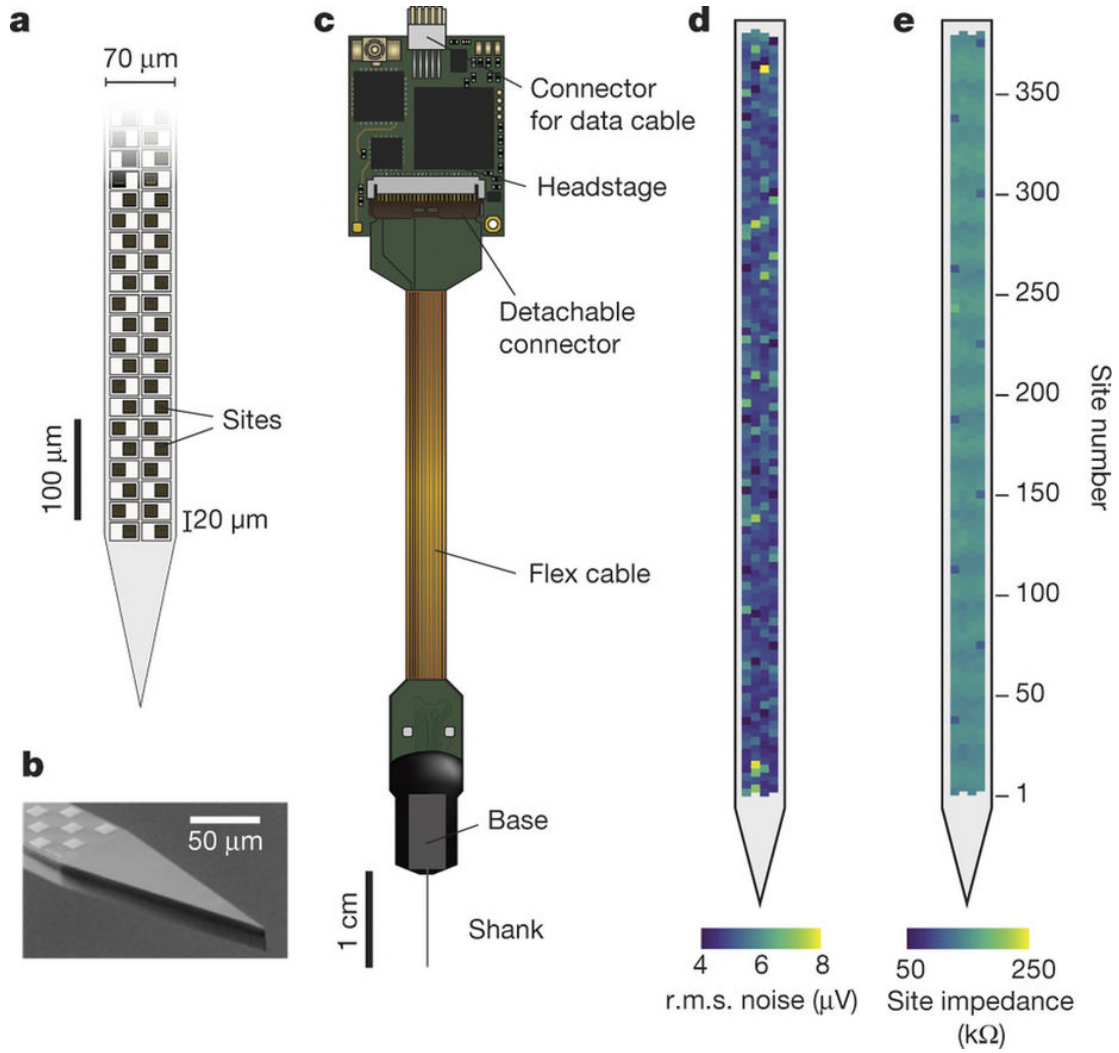

Jun et al., *Nature* 2017

INSIGHT REVIEW NATURE|Vol 461|15 October 2009 |doi:10.1038/nature08540

Electrophysiology in the age of light

Massimo Scanziani[1] & Michael Häusser[2]

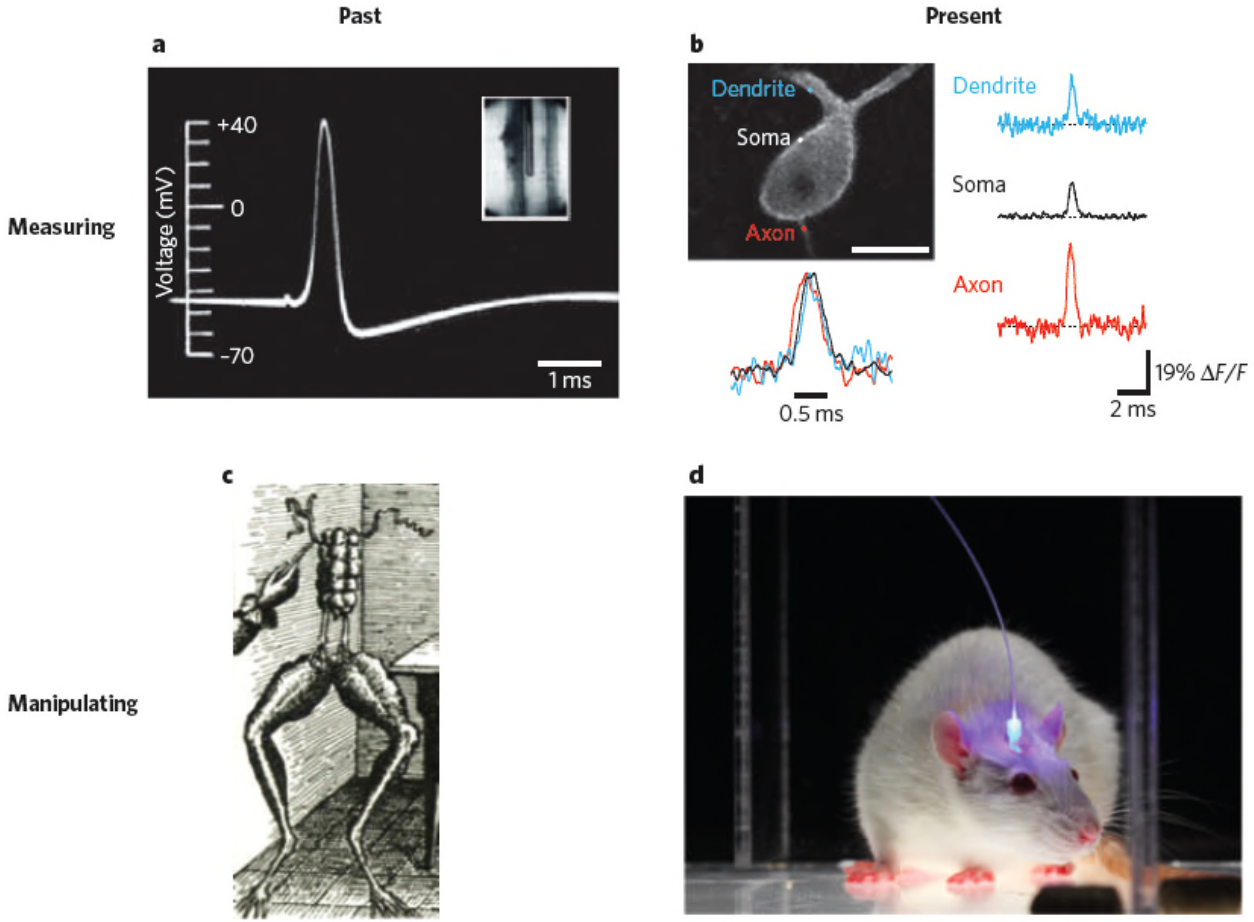

A range of affinities and kinetics

Table 1. Indicator Dissociation Constants for Calcium

İndicator	K_D (µM)	Reference
Fura-2	0.16	(Kao and Tsien 1988)
Magnesium green	7	(Zhao et al. 1996)
Fura dextran (10,000 MW)	0.52	(Konishi and Watanabe 1995)
Calcium green dextran (3,000 MW)	0.54	(Haugland 1996)
Fluo-4 dextran (10,000 MW)	3.1	

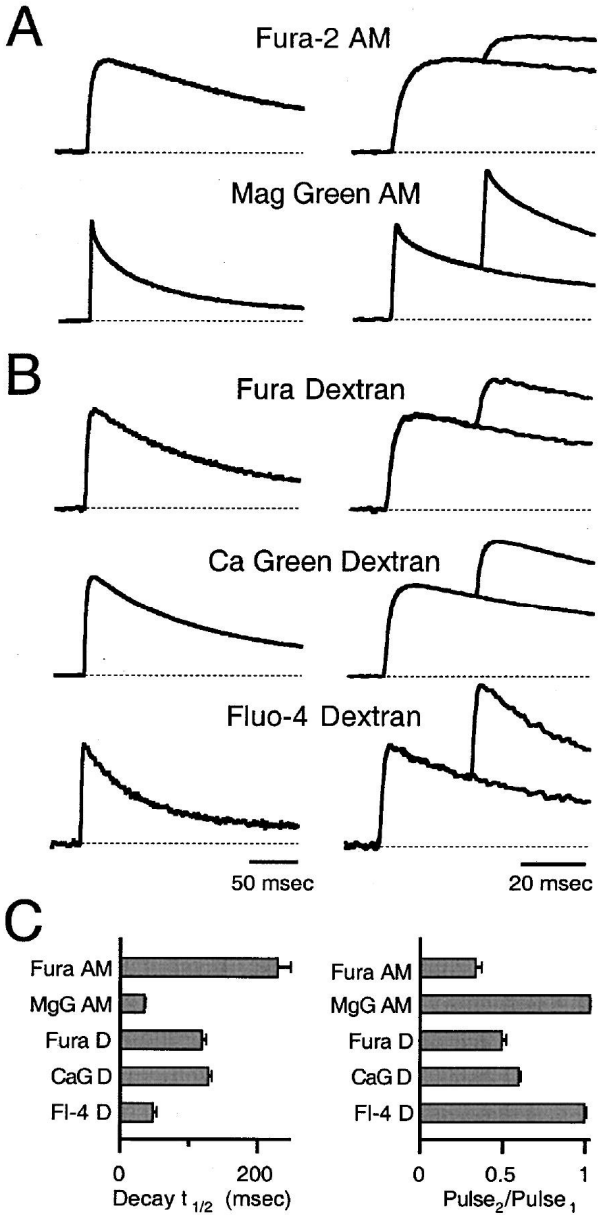

Kreitzer et al., *Neuron* **27**:25 (2000)

Dye imaging from a presynaptic terminal

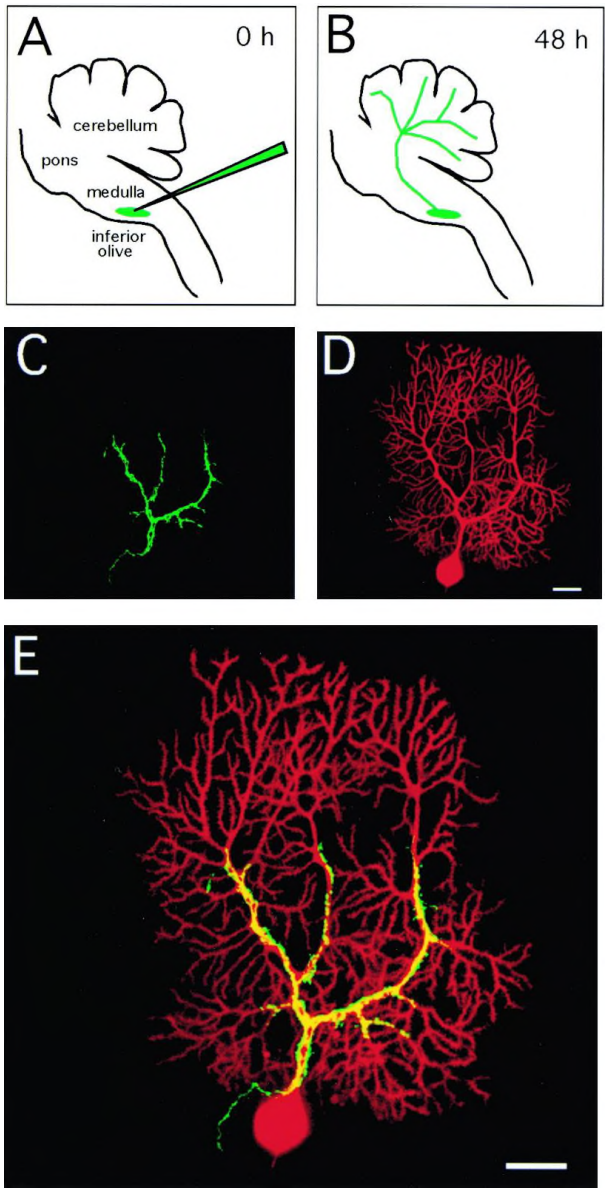

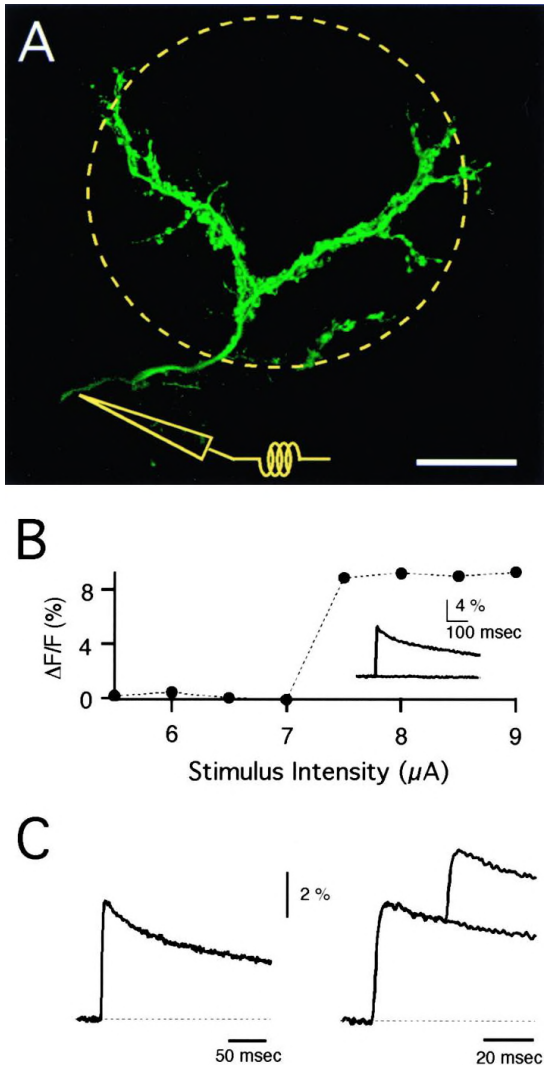

Kreitzer et al., *Neuron* **27**:25 (2000)

Ca^{++} dyes *in vivo*

‘Bulk loading’

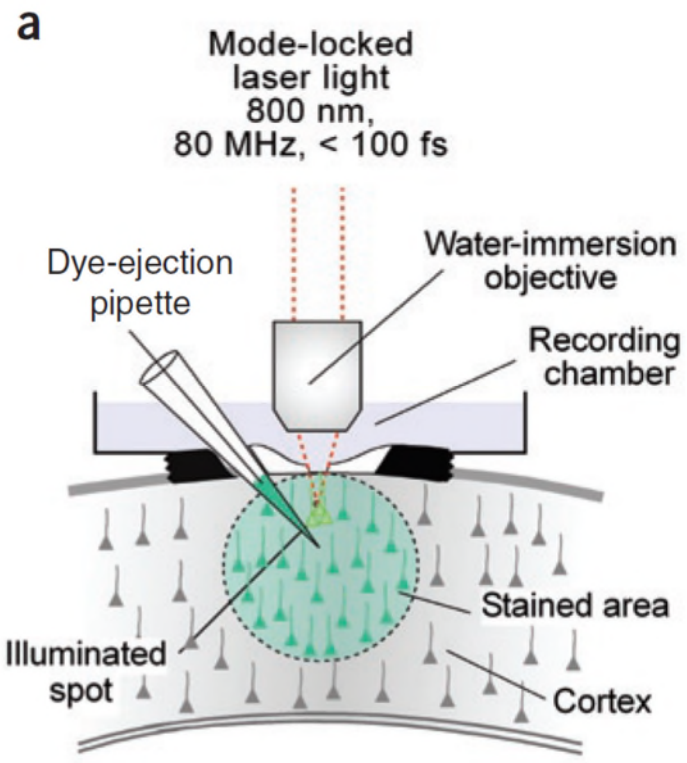

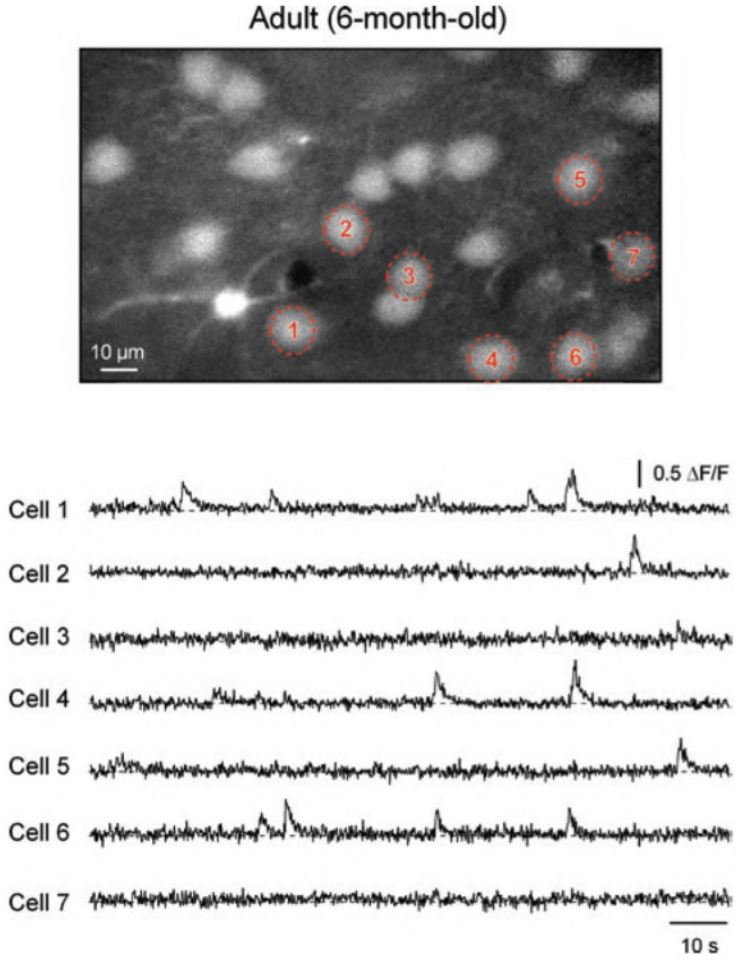

Garaschuk & Konnerth, *Nature Protocols* **1**:380-6, 2006

Optogenetic *sensors* and *actuators*

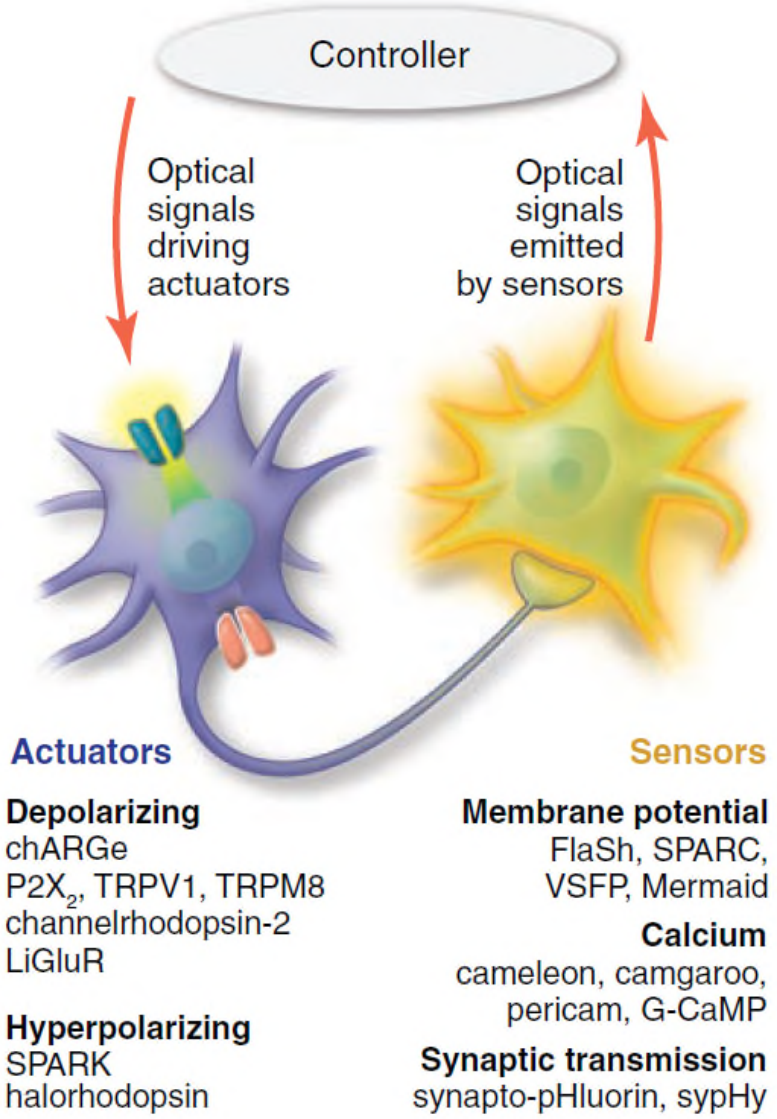

Miesenböck, *Science*, 2009

A revolution in biotechnology caused by a protein from a jellyfish

Green fluorescent protein

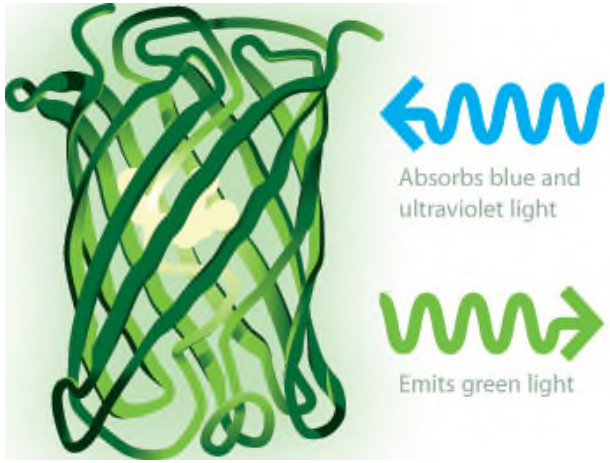

2008 Nobel prize in Chemistry: Shimomura, Chalfie, & Tsien

Fundamentals of fluorescence

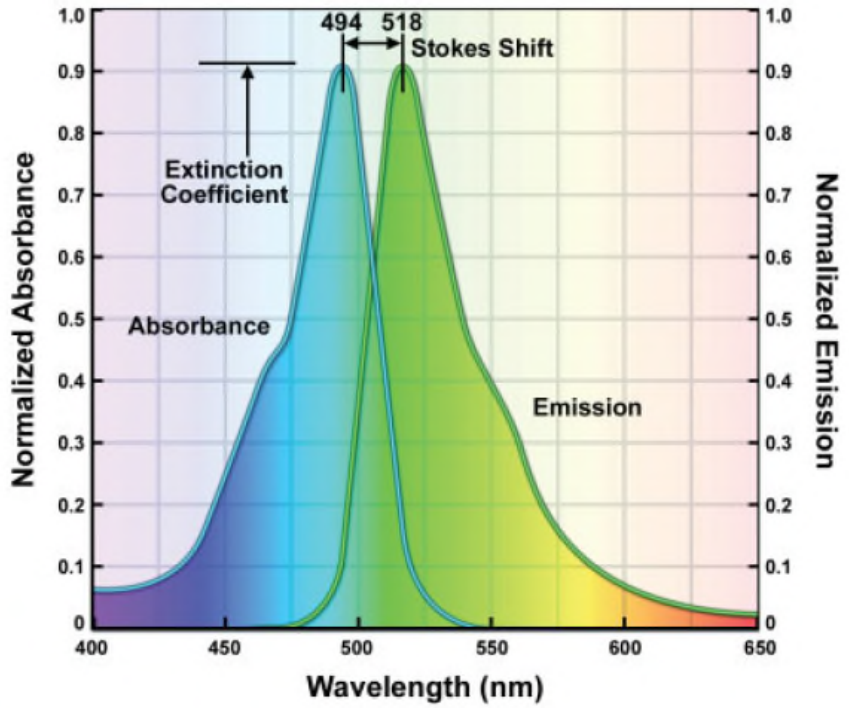

Figure 11.3

Normalized absorption and fluorescence emission spectra of fluorescein conjugated to IgG. Both spectra span a wide range of wavelengths. Fluorescein has an absorption/excitation peak at 494 nm and looks yellow-green to the eye, but actually fluoresces at wavelengths ranging from blue to red with a peak at 518 nm. The difference in nanometers between the excitation and emission maxima is called the Stokes shift. The molar extinction coefficient is measured at the peak of the absorbance spectrum as indicated in the figure.

From Ch.11, *Fundamentals of Light Microscopy and Electronic Imaging*, 2nd Ed., Murphy & Davidson

Multicolored fluorescent proteins

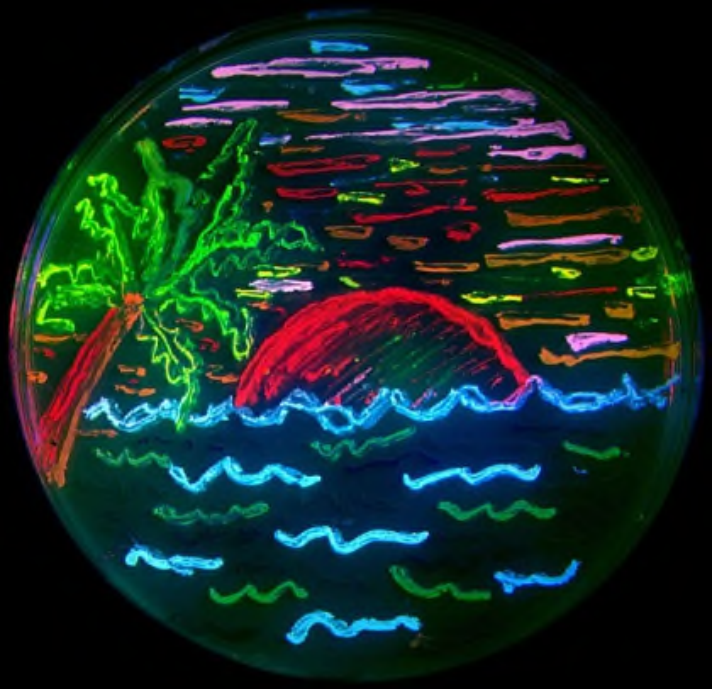

TABLE 11.2 Physical Properties of Useful Fluorescent Proteins

Protein[a]	Color[b]	Excitation (nm)	Emission (nm)	Brightness[c]	Photostability[d]	Filter Set[e]
EBFP2	Blue	383	448	18	++	DAPI
mCerulean	Cyan	433	475	17	++	CFP
mTurquoise	Cyan	433	474	25	+++	CFP
mTFP1	Teal	462	492	54	+++	CFP
mEGFP	Green	488	507	34	++++	FITC/GFP
mEmerald	Green	487	509	39	++++	FITC/GFP
mVenus	Yellow	515	528	53	++	FITC/YFP
mCitrine	Yellow	516	529	59	++	FITC/YFP
mKO2	Orange	551	565	40	+++	TRITC
tdTomato	Orange	554	581	95	+++	TRITC
TagRFP	Orange	555	584	48	++	TRITC
mApple	Orange	568	592	37	+++	TRITC
mCherry	Red	587	610	17	+++	TxRed
mKate2	Far-Red	588	633	25	++	TxRed
mPlum	Far-Red	590	649	3.2	+++	TxRed
mNeptune	Far-Red	600	650	13	++++	Cy5

[a] Common literature abbreviation.
[b] Spectral class.
[c] Product of the molar extinction coefficient and the quantum yield $(mM \times cm)^{-3}$.
[d] Relative to mEGFP (++++).
[e] Recommended filter set.

From Murphy and Davidson, Ch 11

Circularly-permuted GFP and ‘CAMgaroo’

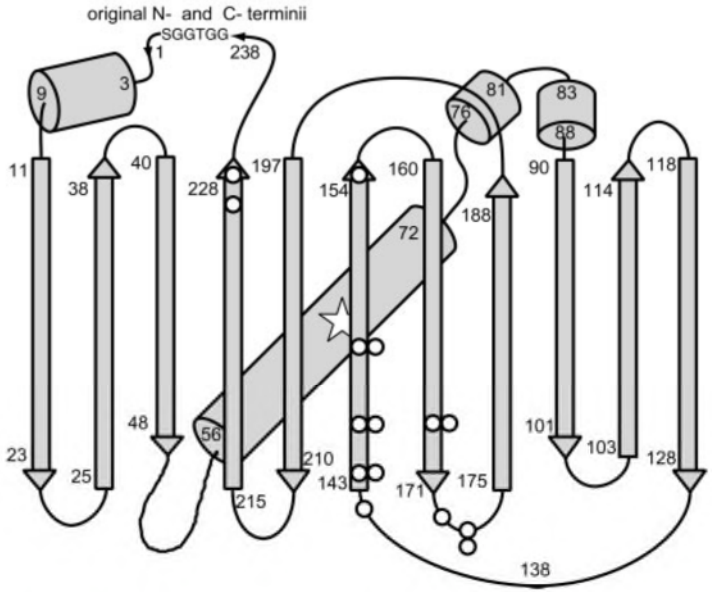

FIG. 2. Schematic drawing of the overall fold of GFP (12) modified to show starting points of fluorescent circular permutations (○), the linker (GGTGGS) connecting the original N and C termini, and the approximate location of the chromophore (open star, residues 65–67). Locations with two circles indicate where circular permutations with two different ending amino acids were isolated (Table 1).

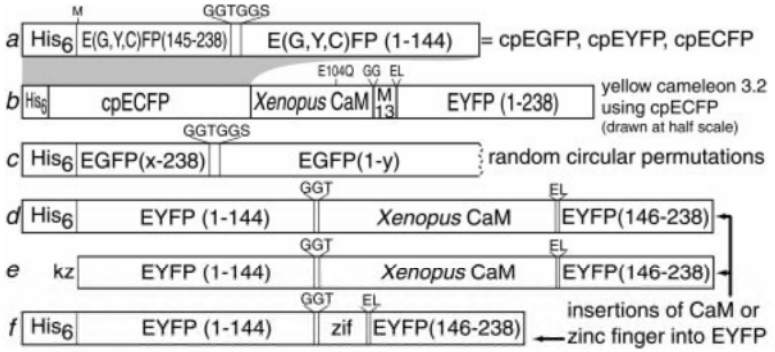

FIG. 1. Schematic structures of major new constructs. (*a*) Designed circular permutations of EGFP, EYFP, and ECFP starting at Y145M. His_6 indicates the polyhistidine tag MRGSHHHHHHGMASMTG-GQQMGRDLYDDDDKDP. Linkers and substitutions are shown above the main sequence. (*b*) Yellow cameleon 3.2 (YC3.2) incorporating cpECFP instead of ECFP. This sequence is drawn at half the scale of all the other constructs. M13 is the CaM-binding peptide derived from skeletal muscle myosin light chain kinase (7). (*c*) Random circular permutations of EGFP. The successful values of *x* and *y* are shown in Table 1. (*d* and *e*) Insertions of CaM in place of Y145 of EYFP as expressed in bacteria (*d*) for *in vitro* purification or in HeLa cells (*e*) for *in situ* monitoring of cytosolic Ca^{2+}. kz, Kozak sequence (10) for optimal translation initiation. (*f*) Insertion of a zinc finger (zif), residues 334–362 of zif268 (8), in place of Y145 of EYFP.

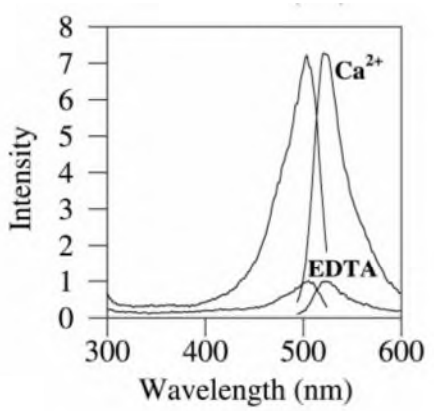

An apt nickname for this construct is ‘‘camgaroo1,’’ because it is yellowish, carries a smaller companion (calmodulin) inserted in its ‘‘pouch,’’ can bounce high in signal, and may spawn improved progeny.

Baird et al., *PNAS* **96**:11241-46, 1999

The GCaMP family of calcium sensors

GCaMP1 described in 2001:
Nakai et al.,, *Nat. Biotech.* 19:137

GCaMP6:
Chen et al., 2013
Nature, 499:295

See also B-GECO and
R-GECO

crystal structure of GCaMP2:
Akerboom et al., *JBC* 284:6455, 2009

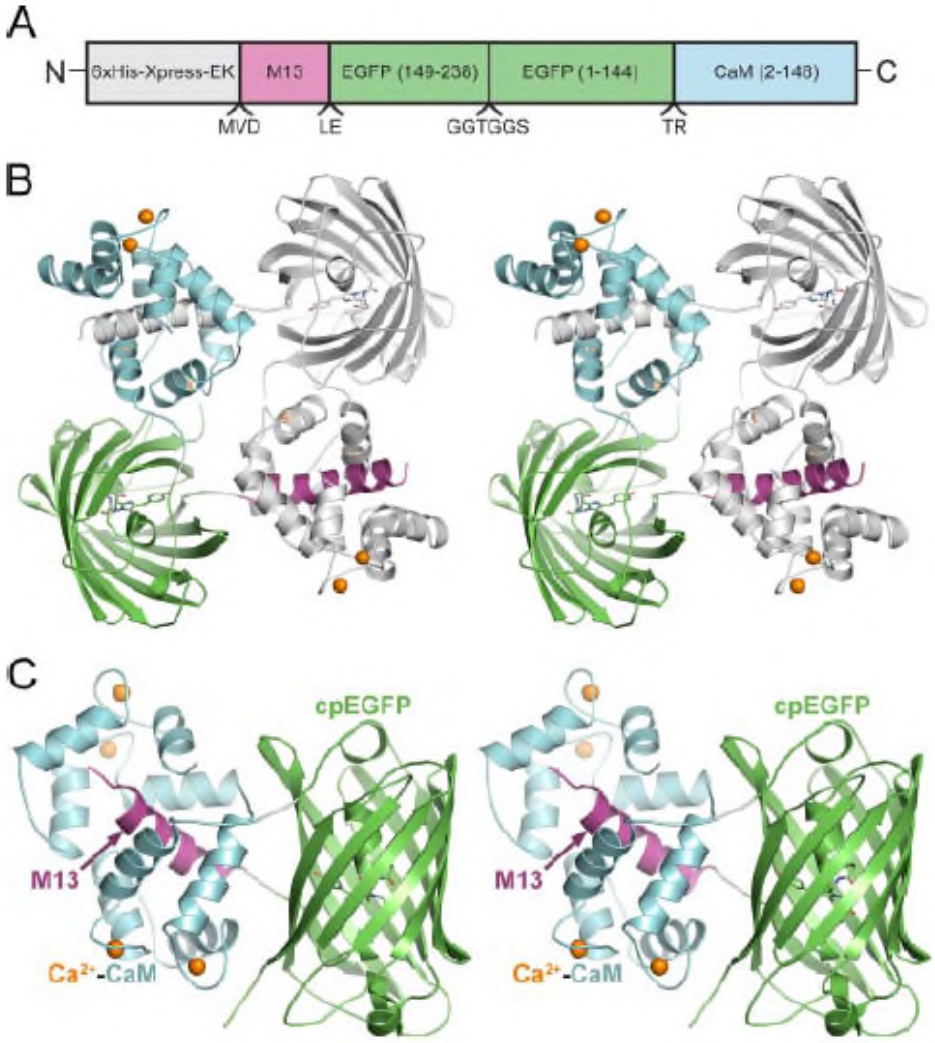

Imaging place cells while the mouse navigates a virtual reality maze

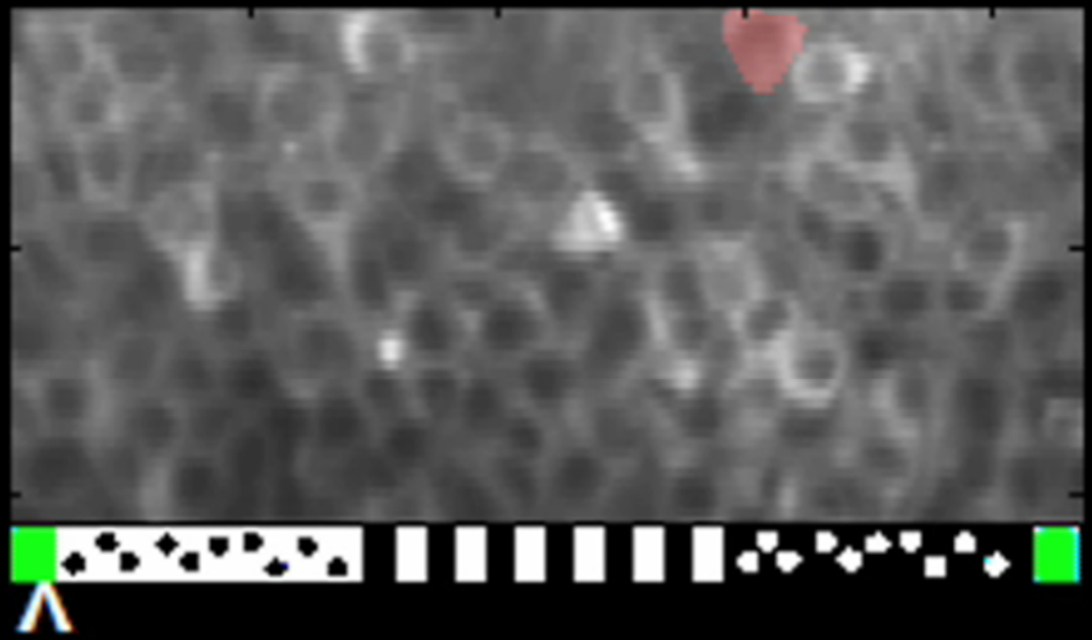

- GCaMP3
- CA1 region

Dombeck et al., *Nature Neuroscience* 13:1433, 2010

Optical sensors of voltage

Genetically encoded voltage sensing strategies

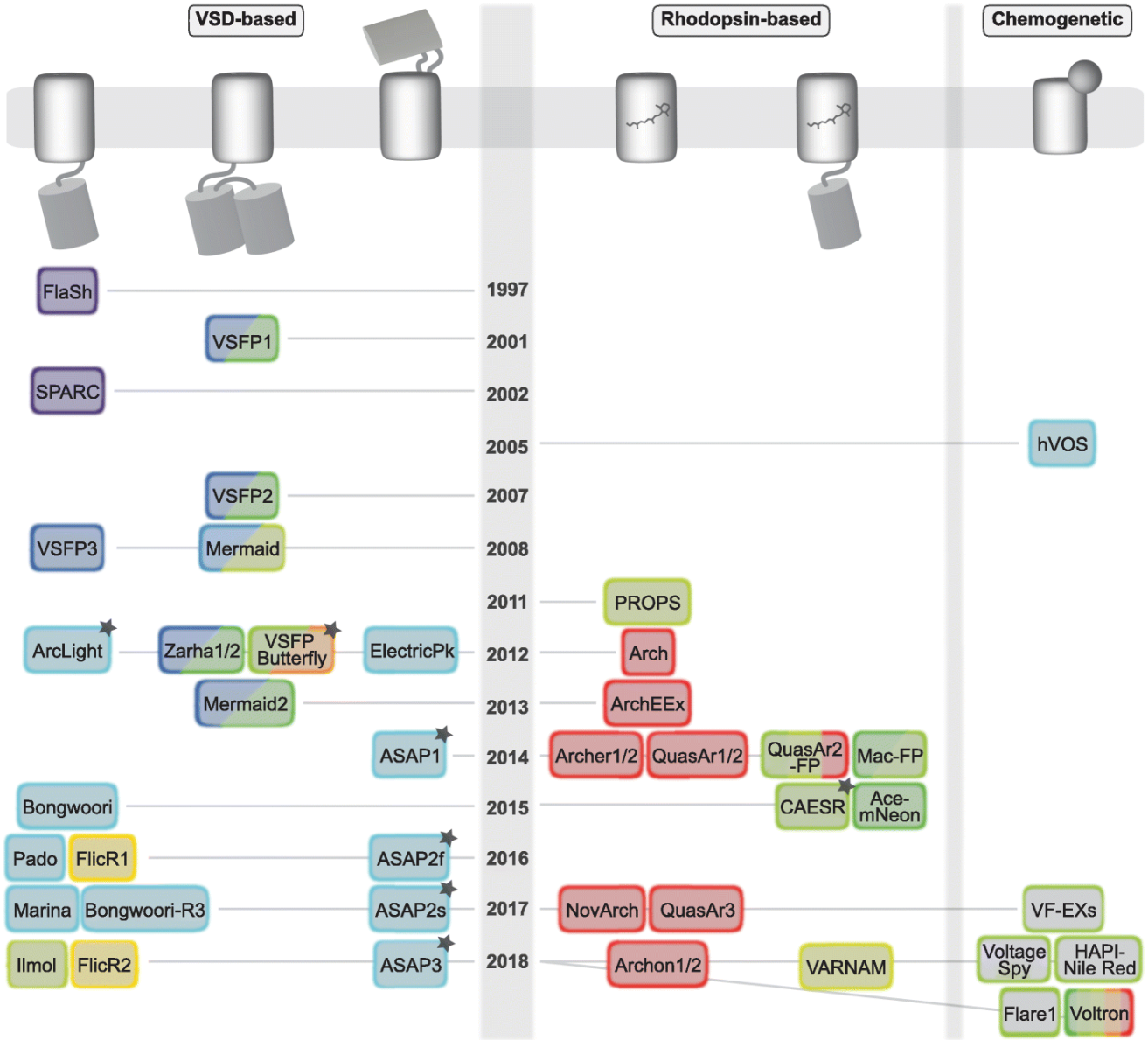

Bando et al., *BMC Biology*, **17**:71, 2019

All of the genetically-encoded voltage sensors compared…

Table 1 Comparative performance of genetically targeted voltage indicators. Values extracted from the literature. *NR* not reported, *RT* room temperature

	λ_{ex} [nm]	λ_{em} [nm]	Rise time (depol.) [ms]	Decay time (hyperpol.) [ms]	Intensity ~[W/cm^2]	SNR	Res. spike rate [Hz]	$\Delta F/F$ for 100 mV	Bleaching	Reference
VSD-based										
ArcLight Q239	480	520	τ_1 = 9 (50%) τ_2 = 48 (RT)	τ_1 = 17 (79%) τ_2 = 63 (RT)	Xenon arc lamp	3.7 per AP	10	−35%	τ = 244 s	Jin 2012 [34]; Bando 2019 [49]
ArcLight-MT	480	535	τ = 84.8 (RT)	τ = 91.9 (RT)	Mercury arc lamp	5.6 per AP	10	−20%	τ = 360 s	Kwon 2017 [46]; Bando 2019 [49]
ASAP1	472	525	τ_1 = 2.1 (60%) τ_2 = 71.5 (RT)	τ_1 = 2.0 (43.7%) τ_2 = 50.8 (RT)	10^{-1}	14.6 per AP	200	− 20%	τ = 35 m	St-Pierre 2014 [38]
ASAP2f	470	525	τ_1 = 2.8 (81%) τ_2 = 135 (RT)	τ_1 = 2.4 (71%) τ_2 = 155 (RT)	10^0	5 per AP	100	−20%	τ = 404 s	Yang 2016 [39]; Chamberland 2017 [41]
ASAP2s	480	525	τ_1 = 5.2 (56%) τ_2 = 63 (RT)	τ_1 = 24 (49%) τ_2 = 106 (RT)	10^0	8 per AP	100	−38%	τ_1 = 121 s (69%) τ_2 = 1017 s	Chamberland 2017 [41]
ASAP3	484	525	τ_1 = 3.7 (81%) τ_2 = 48 (RT)	τ_1 = 16 (81%) τ_2 = 102 (RT)	10^{-1}	2.6 per AP (2P)	100	−50%	19.6%/first 10 s 0.99%/m after that (2P)	Chavarha 2018 [40]
Bongwoori	472	496	τ_1 = 8 (91%) τ_2 = 30 (RT)	τ = 7 (RT)	Xenon arc lamp	19 per AP	60	−15%	> 450 s	Piao 2015 [37]; Lee 2017 [91]
Bongwoori-R3	472	497	τ_1 = 7 (90%) τ_2 = 45 (RT)	τ_1 = 6 (91%) τ_2 = 46 (RT)	Xenon arc lamp	52 per AP	65	−20%	> 450 s	Lee 2017 [91]
FlicR1	561	595	τ_1 = 3 (90%) τ_2 = 42 (RT)	τ_1 = 2.8 (70%) τ_2 = 18 (RT)	10^1	6 per AP	100	6.40%	τ = 150 s	Abdelfattah 2016 [42]; Kannan 2018 [44]
FlicR2	561	630	τ_1 = 2.9 τ_2 = 29.5 (RT)	τ_1 = 3.1 τ_2 = 28.5 (RT)	10^0	NR	NR	12.90%	NR	Kannan 2018 [44]
Marina	488	520	τ = 29.2 (RT)	τ_1 = 15.6 (61%) τ_2 = 59.4 (RT)	10^0	4.5 per AP	NR	29.20%	τ = 206 s	Platisa 2017 [43]
Mermaid	455	480 (donor) 575 (acceptor)	τ_1~ 12 τ_2~200 (RT)	τ~ 128 (RT)	10^0	NR	100	~30% $\Delta R/R$	NR	Tsutsui 2008 [28]
VSFP Butterfly1.2	483	542 (donor) 594 (acceptor)	τ_1~1.5 (35%) τ_2~15 (RT)	NR	Xenon arc lamp	NR	40	5% $\Delta R/R$	NR	Akemann 2012 [92]
Rhodopsin-based										
Arch	640	687	< 1	< 1	10^3	NR	NR	40% at 640 nm	NR	Kralj 2012 [29]; Maclaurin 2013 [58]; Hochbaum 2014 [93]
Arch (D95N)	640	687	τ_1 = 0.5 (20%) τ_2 = 41 (RT)	NR	10^3	NR	NR	50% at 640 nm	NR	Kralj 2012 [29]; Maclaurin 2013 [58]
Archer1	655	NR	Like Arch	Like Arch	10^2	NR	40	85% at 655 nm	NR	Flytzanis 2014 [53]
QuasAr1	640	715	τ_1 = 0.05 (94%) τ_2 = 3.2 (RT)	Similar to rising	10^2	20–30 per AP	NR	32% at 640 nm	τ = 440 s	Hochbaum 2014 [93]

Table 1 Comparative performance of genetically targeted voltage indicators. Values extracted from the literature. *NR* not reported, *RT* room temperature *(Continued)*

	λ_{ex} [nm]	λ_{em} [nm]	Rise time (depol.) [ms]	Decay time (hyperpol.) [ms]	Intensity ~[W/cm^2]	SNR	Res. spike rate [Hz]	$\Delta F/F$ for 100 mV	Bleaching	Reference
QuasAr2	640	715	τ_1 = 1.2 (68%) τ_2 = 11.8 (RT)	Similar to rising	10^2	40–70 per AP	NR	90% at 640 nm	τ = 1020 s	Hochbaum 2014 [93]
QuasAr3	Like QuasAr2	Like QuasAr2	τ_1 = 1.2 (77%) τ_2 = 10.0 (34 °C)	τ_1 = 0.9 (91%) τ_2 = 9.0 (34 °C)	10^2	27 per AP	NR	54% at 640 nm	NR	Adam 2018 [55]
Archon1	637	NR	τ_1 = 0.6 (88%) τ_2 = 8.1 (34 °C)	τ_1 = 1.1 (88%) τ_2 = 13 (34 °C)	10^1–10^2	21 per AP	NR	43% at 637 nm	0.01%/s	Piatkevich 2018 [57]
Archon2	637	NR	τ_1 = 0.6 (70%) τ_2 = 6.7 (34 °C)	τ_1 = 0.17 (92%) τ_2 = 7.0 (34 °C)	10^1–10^2	16 per AP	200	19% at 637 nm	0.03%/s	Piatkevich 2018 [57]
QuasAr2-mOrange	549	565	τ_1 = 3.9 (60%) τ_2 = 27 (23 °C)	τ_1 = 4.3 (45%) τ_2 = 26 (23 °C)	10^1	9 per AP	NR	−10%	NR	Zou 2014 [61]
MacQ-mCitrine	515	530	τ_1 = 2.8 (74%) τ_2 = 71 (RT)	τ_1 = 5.4 (77%) τ_2 = 67 (RT)	10^1	NR	NR	−20%	1.3%/s	Gong 2014 [60]; Gong 2015 [52]
Ace2-4aa-mNeon	505	515	τ_1 = 0.37 (58%) τ_2 = 5.5 (RT)	τ_1 = 0.5 (60%) τ_2 = 5.9 (RT)	10^1	NR	NR	−12%	0.6%/s	Gong 2015 [52]
VARNAM	558	605	τ_1 = 0.88 τ_2 = 5.2 (RT)	τ_1 = 0.80 τ_2 = 4.7 (RT)	10^1	36 per AP	100	−14% for 120 mV	τ = 256 s	Kannan 2018 [44]
Chemogenetics based										
hVOS	480	535	< 1	< 1	Mercury arc lamp	NR	667	34%	NR	Chanda et al. 2005 [70]
Flare1	488	570	τ_1 = 0.92 (96%) τ_2 = 23.5	τ_1 = 1.41 (91%) τ_2 = 25.6	10^0	53	20	35.9%	NR	Xu et al. 2018 [74]
Voltron 525	532	553	τ_1 = 0.64 (61%) τ_2 = 4.1	τ_1 = 0.78 (55%) τ_2 = 3.9	10^0	4.4	10	30%	τ = 206 s	Abdelfattah 2016 [42]
VF-EX	525	540	< 1	< 1	NR	20	3	21%	NR	Liu et al. 2017 [77]
VoltageSpy	525	540	< 1	< 1	10^{-1}–10^0	7.7	NR	60%	NR	Grenier et al. 2019 [82]
HAPI-Nile	540–552	581	τ_1 = 1.9 (85%)	τ_1 = 1.9 (85%)	10^1	12.4	10	5.50%	NR	Sundukova et al. 2019 [83]

Bando et al., *BMC Biology*, 2019

ASAP1, a VSD-based indicator using a circularly permuted GFP

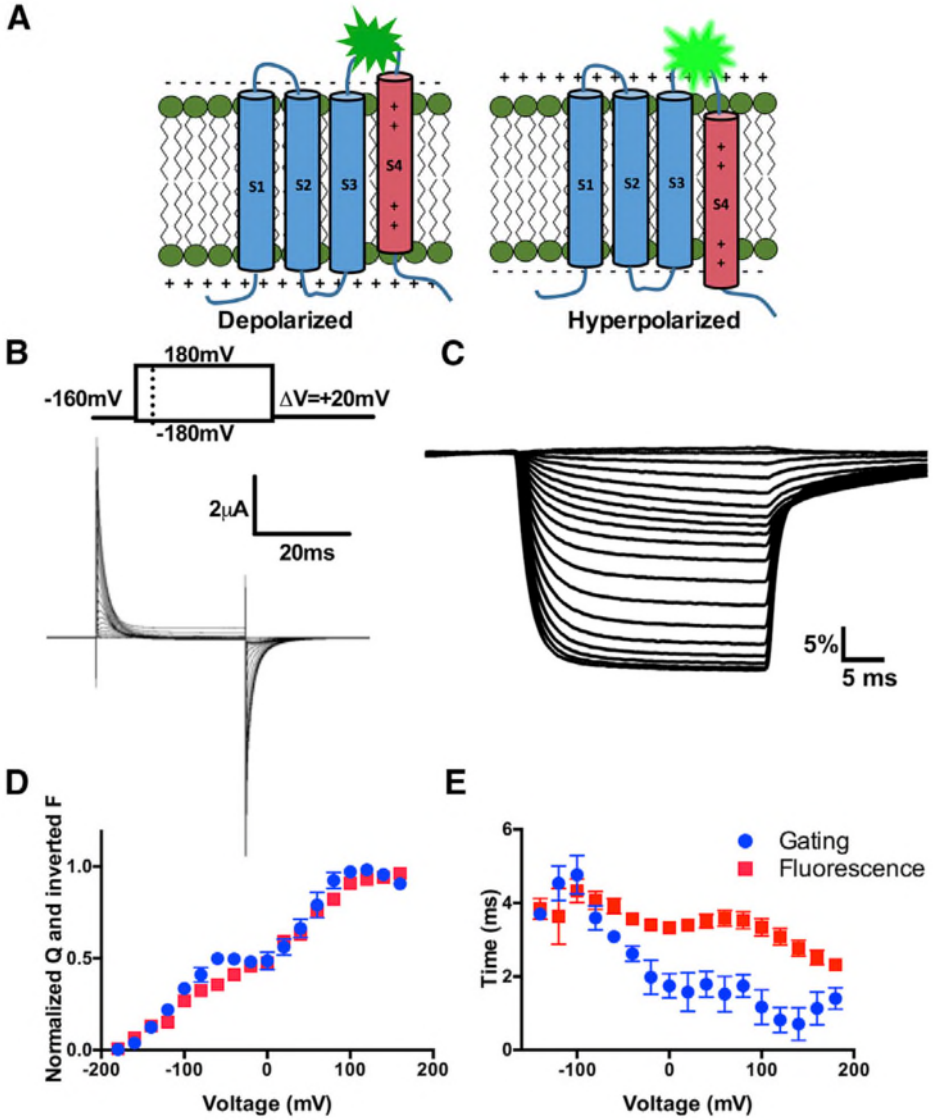

Lee & Bezanilla, *Biophys. J.* **113**:2178-81, 2017

Archaerodopsin 3, a rhodopsin-based voltage indicator - fast but low QY and super dim

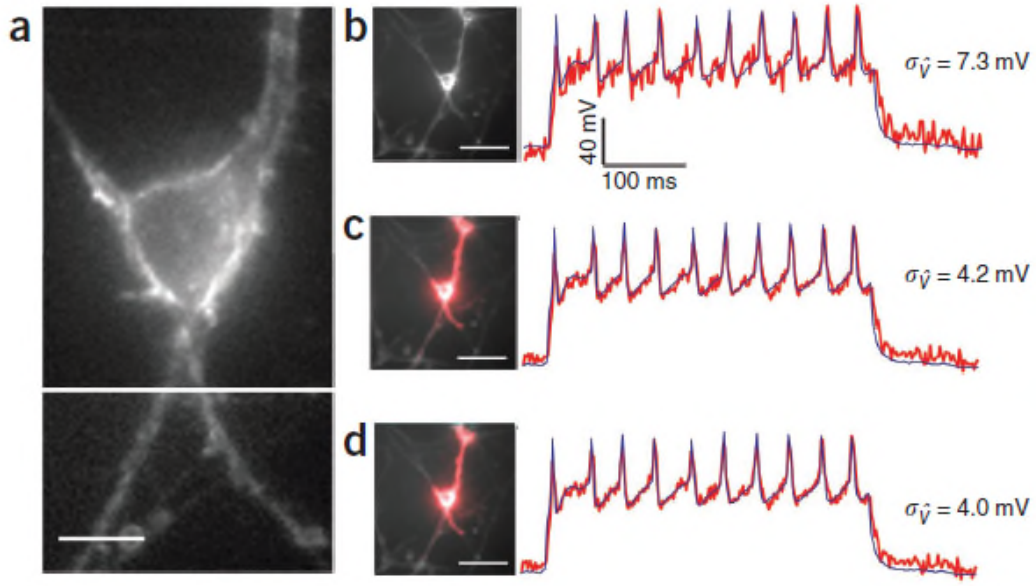

Kralj et al., *Nat. Methods*, **9**:90, 2011

Table 1 | Optical and electrical response of Arch and Arch(D95N)

	λ_{max} absorbance (nm)	λ_{max} emission (nm)[a]	ε_{633} (M^{-1} cm^{-1})[b]	QY[c]	Photostability relative to eGFP[d]	pK_a of Schiff base[e]	$\tau_{response}$ (ms)[f]	Noise in $\tilde{V}_{FL}$ (μV $Hz^{-0.5}$)[g]	Photo-current
Arch	558	687	6,300	9×10^{-4}	0.25	10.1	<0.5	625	Yes
Arch(D95N)	585	687	37,500	4×10^{-4}	0.1	8.9	41	260	No

A non-genetic voltage sensor that relies on FRET-based quenching

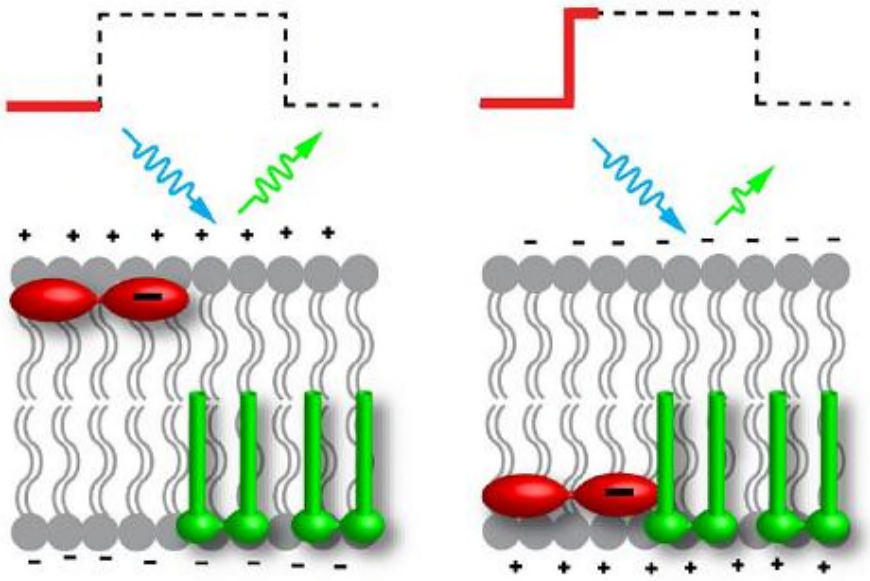

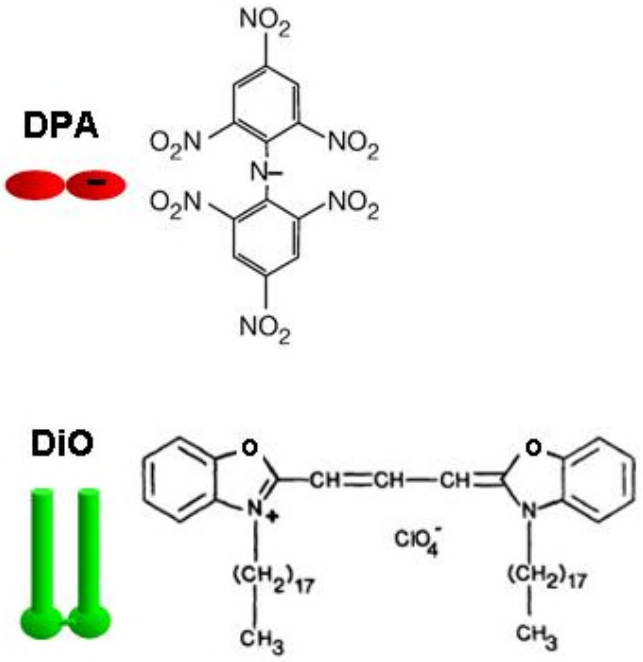

Bradley et al., *J. Neurosci.*, 2009

Two photon compatibility, high SNR

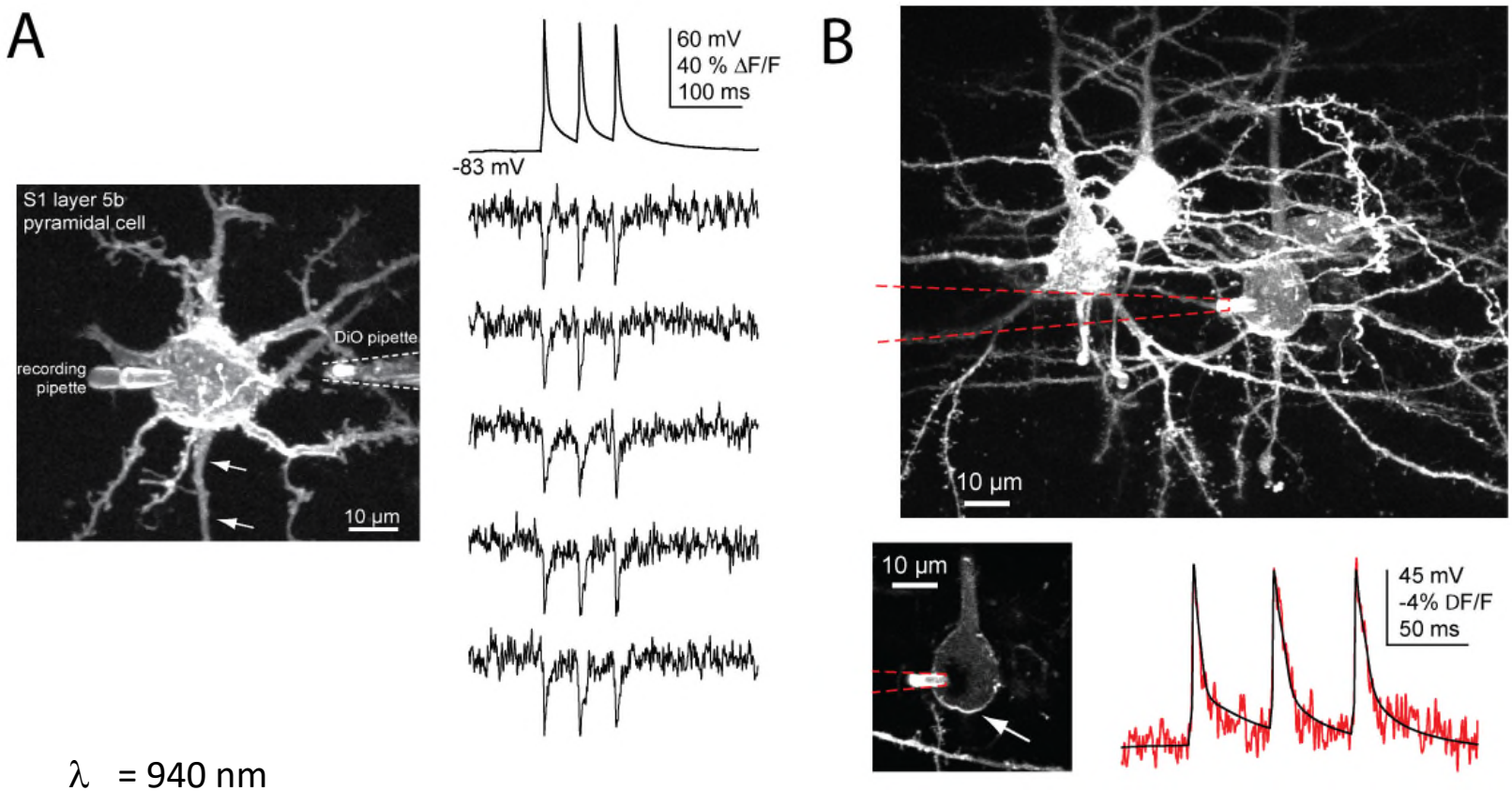

λ = 940 nm
3 µM DPA

Fink et al., PLOS One, 2012

Voltron, a ‘modular’ chemogenetic-based voltage sensor

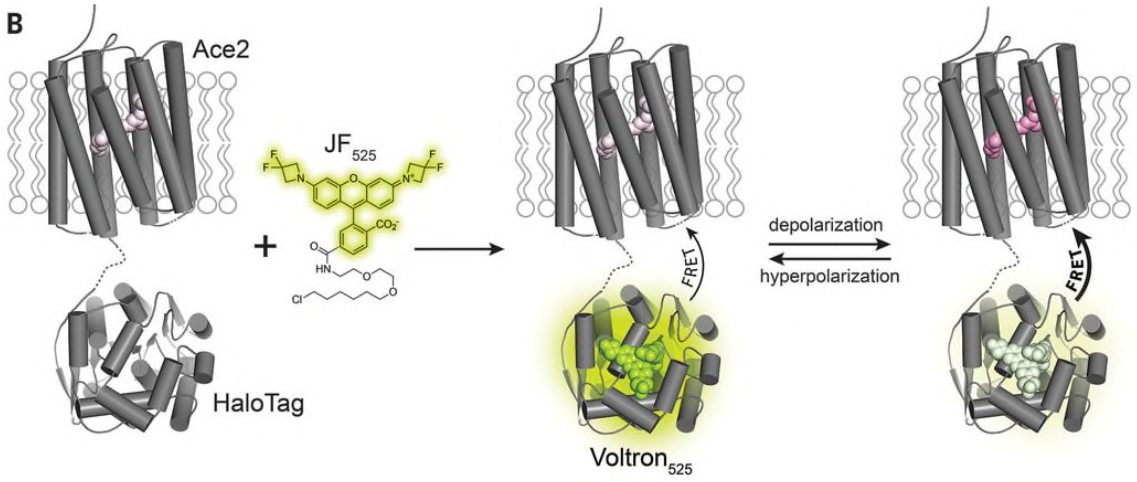

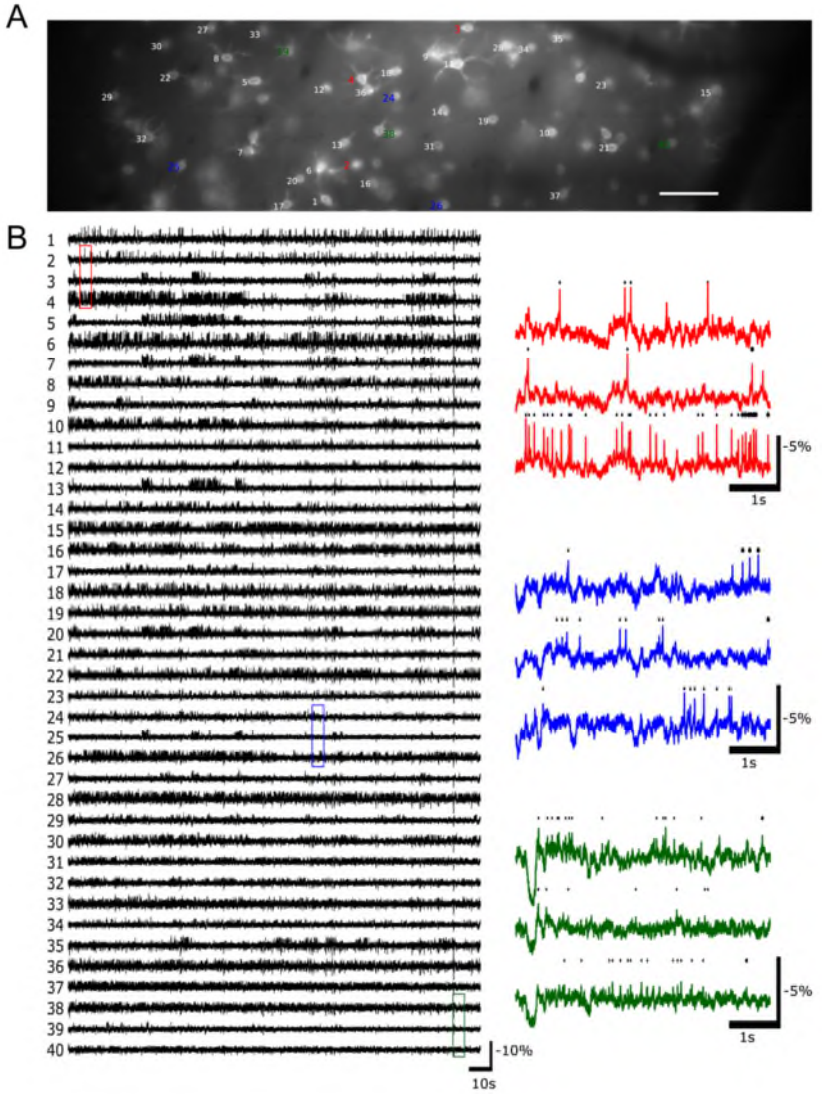

Abdelfattah et al., *Science* 2019

Essential things to consider in comparing GEVIs

photophysical properties

- QY, brightness
- 2P compatibility
- kinetics
- SNR
- bleaching
- linearity

ease of expression, protein trafficking

- if it's not in the PM its background

other liabilities

- tolerance/side effects for chemo-based
- capacitive load for VSD-based

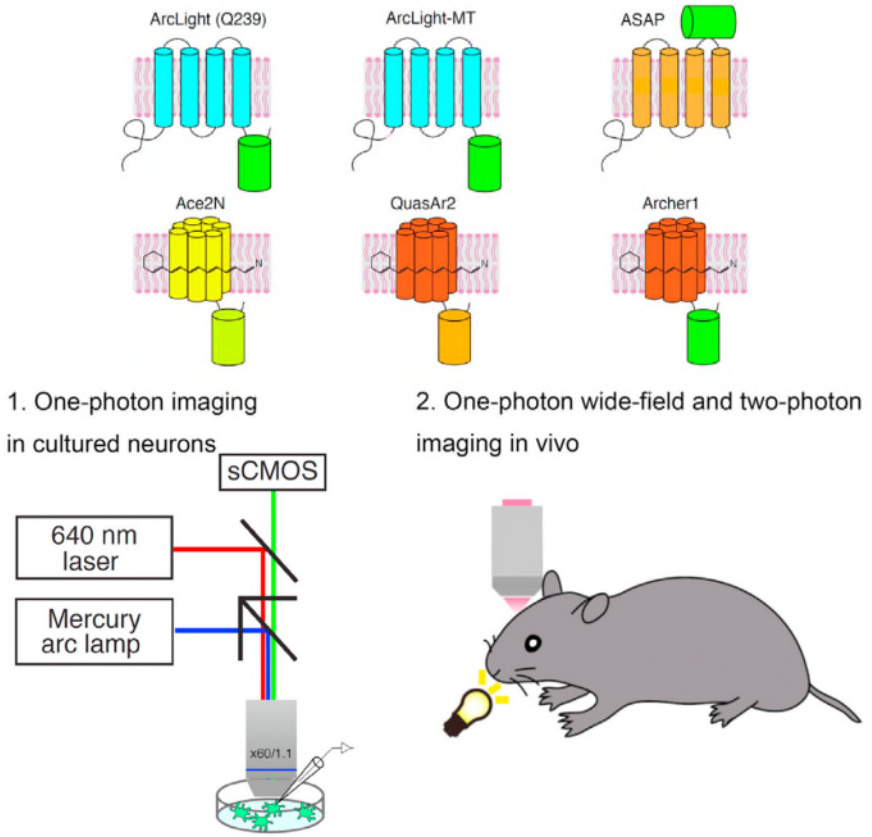

Bando et al., *Cell Reports*, 2019
See also Box 1 from Bando et al, *BMC Biology*, 2019

Unfinished Marx-Engels sculpture at Ludwig Engelhardt's studio in Gummlin, Usedom, Sybille Bergemann, 1984

Backup/extra

Conditional genetics and lab mice

Breeding strategy

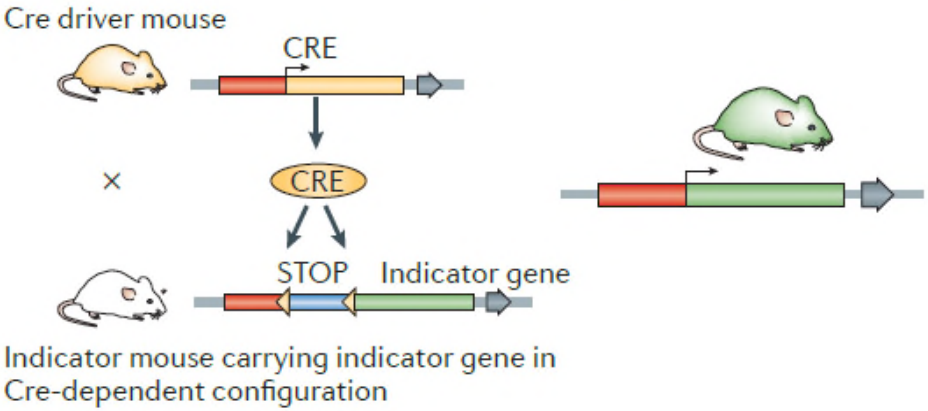

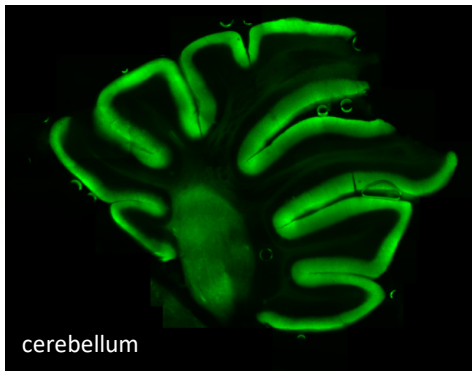

Viral strategy

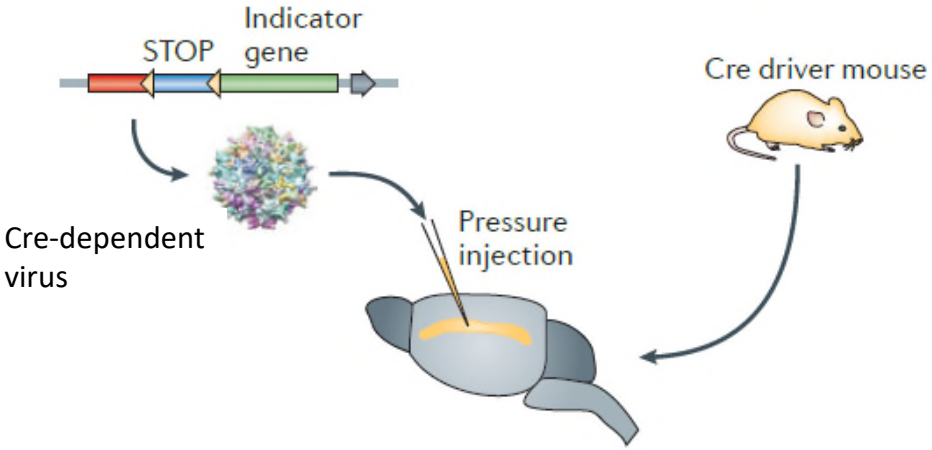

from Knopfel,
Nat. Rev. Neurosci.
2012

CAMPARI, a conditional integrator of neural activity

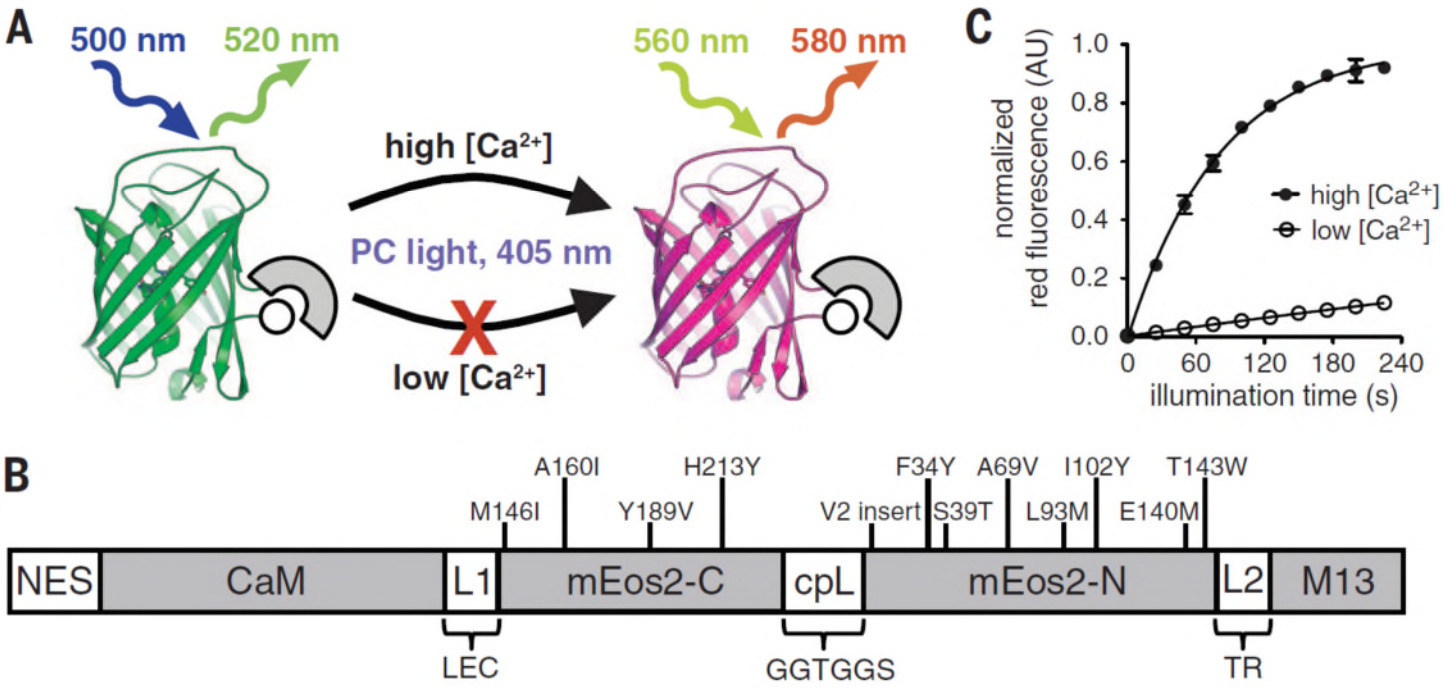

Fusque et al. *Science*, **347**:755-60, 2015